JGR Planets

RESEARCH ARTICLE
10.1029/2020JE006791

Lava Flow Eruption Conditions in the Tharsis Volcanic Province on Mars

S. I. Peters[1], **P. R. Christensen**[1], **and A. B. Clarke**[1,2]

[1]School of Earth and Space Exploration, Arizona State University, Tempe, AZ, USA, [2]Istituto Nazionale di Geofisica e Vulcanologia, Pisa, Italy

Key Points:

- The large thick lava flows in Tharsis are explained by basaltic and basaltic-andesite compositions without resorting to exotic compositions
- The observed lava flows likely required longer-lived eruptive conditions and larger active conduits than their terrestrial counterparts
- Seemingly high eruption rates for some solitary flows are reasonable extrapolations of terrestrial conditions with higher supply dimensions

Supporting Information:

Supporting Information may be found in the online version of this article.

Correspondence to:

S. I. Peters,
speter24@asu.edu

Citation:

Peters, S. I., Christensen, P. R., & Clarke, A. B. (2021). Lava flow eruption conditions in the Tharsis volcanic province on Mars. *Journal of Geophysical Research: Planets*, *126*, e2020JE006791. https://doi.org/10.1029/2020JE006791

Received 30 NOV 2020
Accepted 21 JUN 2021

Author Contributions:

Funding acquisition: P. R. Christensen
Methodology: A. B. Clarke
Resources: P. R. Christensen, A. B. Clarke
Supervision: P. R. Christensen, A. B. Clarke
Writing – review & editing: P. R. Christensen, A. B. Clarke

Abstract Volcanism has played a major role in modifying the Martian surface. The Tharsis volcanic province dominates the western hemisphere of the planet with numerous effusive volcanic constructs and deposits. Here, we present the results of an in-depth study aimed at characterizing and modeling the emplacement conditions of 40 lava flows in the Tharsis volcanic province. These lava flows display a range of lengths (~15–310 km), widths (~0.5–29 km), and thicknesses (~11–91 m). The volumes and flow masses range from ~1 to 440 km^3 and ~10^{11} to 10^{14} kg, respectively. Using three different models, we calculated a range of eruption rates (0.3–3.5 × 10^4 m^3/s), viscosities (10^4–10^7 Pa s), yield strengths (800–10^4 Pa), and emplacement times (8 h–11 years). While the flow lengths and volumes are typically larger than terrestrial lava flows by an order of magnitude, rheologies and eruption rates are similar based on our findings. Emplacement times suggest that eruptions were active for long periods of time, which implies the presence and persistence of open subsurface pathways. Differences in flow morphology and emplacement conditions across localities within Tharsis highlight different pathways and volumes of available material between the central volcanoes and the plains. The scale of the eruptions suggests there could have been eruption-driven local, regional, and perhaps, global impacts on the Martian climate. The relatively recent age of the eruptions implies that Mars has retained the capability of producing significant localized volcanism.

Plain Language Summary Volcanoes have resurfaced a majority of the Martian surface. Understanding the volcanic history of Mars is critical to understanding the evolution of the planet. Lava flows are one of the most common volcanic features on Mars, and numerous examples are present in the Tharsis volcanic province on shield volcanoes and in vast volcanic plains. Using three different approaches, we characterized the eruption conditions of 40 lava flows. In addition, we measured their dimensions and calculated volumes and masses. We observed flow dimensions (e.g., lengths and volumes) larger than typical terrestrial lava flows. Viscosities and yield strengths were similar to terrestrial values; however, effusion rates were generally at the higher end of terrestrial rates. These results indicate that lava flows erupted on Mars did not require exotic compositions or exceptionally high eruption rates to be emplaced. However, this does imply longer eruption times, which requires the existence of long-lived subsurface conduits capable of transporting magma to the surface.

1. Introduction

Volcanism is a fundamental geologic process that has created and shaped the surfaces of the terrestrial planets in our solar system. The volcanic history of a planetary body provides information on its formation and evolution (Carr, 1973, 1974; Greeley & Spudis, 1981; Gregg & Fink, 2000; Pieri et al., 1984; Plescia, 2004; Spudis et al., 2013; Werner, 2009; Wilson & Head, 1983). For Mars, where ~60% of the crust has been resurfaced by effusive volcanism, a variety of volcanic landforms have been preserved at the surface, including vast lava flow plains, sinuous rilles, massive shield volcanoes, cinder cones, and ash shields (Carr, 1974; Greeley & Spudis, 1981; Hauber et al., 2011; Hiesinger et al., 2007; Plescia, 2004; Werner, 2009; Xiao et al., 2012). The bulk of Martian volcanism appears to have occurred early in the planet's history (>3 Ga), with decreasing volcanic fluxes through time (Tanaka et al., 2014; Werner, 2009). Despite an abundance of volcanic features on Mars, the volcanic history of the planet remains complicated due to the lack of global compositional data, the lack of observations while the eruptions were active, and sometimes a lack of analogous terrestrial terrain and processes.

Using flow morphology to estimate eruption conditions has been a goal of terrestrial and planetary volcanology for decades and has fueled a number of studies (e.g., Baloga & Glaze, 2008; Cashman et al., 1998; Fink & Griffiths, 1990; Glaze & Baloga, 2006; Gregg & Fink, 1996; Hauber et al., 2011; Hiesinger et al., 2007; Wilson & Head, 1983). In the absence of direct observations, the eruption conditions and flow properties can be estimated based upon the morphology of preserved deposits. These deposits provide a snapshot into the planet's interior and composition. Previous studies have estimated lava flow eruption rates, viscosities, yield strengths, and emplacement times using combinations of simplified fluid mechanics, numerical models, deposit morphology, and morphometry (e.g., Baloga & Glaze, 2008; Glaze & Baloga, 2006; Glaze et al., 2009; Gregg & Fink, 1996; Griffiths & Fink, 1992; Hauber et al., 2011; Hiesinger et al., 2007).

In this study, we have observed and quantified the morphology and dimensions of 40 lava flows in the Tharsis volcanic province on Mars in order to calculate eruption rates, viscosities, yield strengths, and emplacements times. These 40 lava flows occur in the volcanic plains and in proximity to or on central volcanoes. High resolution images up to 0.25 m/pixel High Resolution Imaging Science Experiment (HiRISE) and digital terrain models at ~50–70 m/pixel (HRSC) have enabled detailed analyses of these lava flows (Jaumann et al., 2007; Malin et al., 2007; McEwen et al., 2007; Keszthelyi et al., 2008). We have applied three lava flow emplacement models that utilize flow morphology and morphometry to constrain eruption rates, rheology, and emplacement times, and compared those results to a wide range of analogous terrestrial data. The suite of models consists of (a) a standard cooling-limited rheologic treatment outlined in Hiesinger et al. (2007), (b) the utilization of the nondimensional parameter Ψ derived from laboratory analog experiments, and (c) the self-replication model outlined in Baloga and Glaze (2008). The calculated volumes, eruption rates, viscosities, and emplacement times are interpreted in terms of their implications for the eruption conditions of relatively recent volcanic activity on Mars and the subsurface pathways that transport magma in the Martian crust. An application of this method to lava flows on other volcanic bodies, such as Io or Venus, could also prove useful.

2. Background

The eruption conditions of lava flows on Mars have implications for understanding its composition, interior, and evolution. The morphology of terrestrial and extraterrestrial lava flows has long been used as a proxy for the eruptive conditions at the time of emplacement (e.g., Baloga & Glaze, 2008; Bleacher, Greeley, Williams, Cave, & Neukum, 2007; Bleacher, Greeley, Williams, Werner, et al., 2007; Carr, 1973, 1974; Cashman et al., 1998; Gregg & Fink, 1996; Griffiths & Fink, 1992; Hauber et al., 2011; Hiesinger et al., 2007; Walker, 1971, 1973; Wilson & Head, 1983). A number of studies have used the morphology and morphometry of lava flows on Mars to estimate effusion rates, viscosities, and yield strengths by applying cooling limited and rheologic models (Bleacher, Greeley, Williams, Cave, & Neukum, 2007; Bleacher, Greeley, Williams, Werner, et al., 2007; Glaze & Baloga, 2006; Hauber et al., 2011; Hiesinger et al., 2007; Wilson & Head, 1983). These studies have necessarily made a variety of simplifying assumptions about lava flow rheology, composition, and environmental conditions during emplacement. Some studies have invoked either exceptional eruption rates never observed in terrestrial lava flows or exotic compositions to explain the very large dimensions of Mars lava flows (e.g., Cashman et al., 1998; Wilson & Head, 1983 and references therein; Garry et al., 2007; Giacomini et al., 2009). These analyses were partly predicated on the following assumptions: the length of lava flows is controlled exclusively or largely by eruption rate; the entire flow front is active at all times with the flow moving as a coherent mass; and/or lava behaves as a Newtonian fluid (Baloga & Glaze, 2008; Baloga et al., 1998; Bruno et al., 1996; Nichols, 1939). Although studies have demonstrated a Newtonian rheology may be assumed for the hot interior of a lava flow, Hulme (1976) demonstrated that the behavior of lava flows on Olympus Mons, Mars, and elsewhere, were better approximated by a Bingham rheology due to the significant yield strength of most lavas, particularly as they propagate and cool. Subsequent studies followed suit (e.g., Baloga & Glaze, 2008; Bruno et al., 1996; Glaze & Baloga, 2006; Hauber et al., 2011; Hiesinger et al., 2007). Recent works have accounted for more complex processes that occur during the emplacement of lava flows such as levee construction and overspills (Baloga & Glaze, 2008; Baloga et al., 1998; Glaze et al., 2009). Most studies aimed at constraining lava composition and effusion rates on Mars have focused on the Tharsis and Elysium volcanic provinces where some of the best-preserved lava flows on the planet are located. Due to dust cover, however, compositional data are sparse to nonexistent in these localities

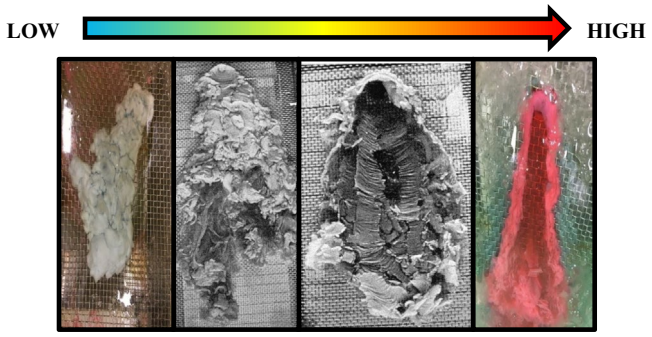

Figure 1. Examples of the four primary morphologies observed by Fink and Griffiths (1990), Gregg and Fink (2000), and Peters (2020). From low to high Ψ, the morphologies are Pillows, Rifts, Folds, and Levees. At very high Ψ, a "no crust" morphology—labeled because a surface crust is not observed for considerable duration of the eruption—is observed. Modified from Gregg and Fink (2000).

(Baloga & Glaze, 2008; Christensen, 1986; Hauber et al., 2011; Hiesinger et al., 2007; Rogers & Christensen, 2007). However, a basaltic-to-basaltic andesite composition of much of the Martian crust has been determined using near IR and thermal infrared spectral measurements of less dust covered regions, although ultramafic terrains have been observed as well (e.g., Jaeger et al., 2010; Rogers & Christensen, 2007). Based on the moderate range of compositions observed in the dust-free regions, it is likely that the Tharsis region is basaltic as well.

Laboratory analog experiments have provided a fundamental understanding of lava flow emplacement processes and their relationship to propagation rate and morphology, and have thus been used to make predictions of lava flow behavior on other planets (Blake & Bruno, 2000; Fink & Griffiths, 1990; Gregg & Fink, 1996, 2000; Griffiths & Fink, 1992; Peters, 2020; Rader et al., 2017; Soule & Cashman, 2004). Previous laboratory studies have examined lava flow morphologies by extruding substances analogous to lava into controlled environments under controlled source conditions (Fink & Griffiths, 1990, 1992; Gregg & Fink, 1996, 2000). Polyethylene glycol (PEG) wax has been demonstrated to be a useful analog to real lava flows due to its temperature dependent viscosity and timescale of surface crust formation (Fink & Griffiths, 1990, 1992; Gregg & Fink, 1996, 2000; Soule & Cashman, 2004). Fink and Griffiths (1990) derived a dimensionless parameter, Ψ, which is a ratio of the characteristic time scale of crust formation, which is controlled by surface cooling, to the characteristic time scale of lateral thermal advection, for which flow propagation rate is a proxy.

Fink and Griffiths (1990) observed five morphologies produced in the laboratory: no crust, levees, folds, rifts, and pillows, which occur on a continuum from high to low Ψ values, respectively (Figure 1). Analogous morphologies have been observed in nature (Fink & Griffiths, 1990, 1992; Gregg & Fink, 1996; Griffiths & Fink, 1992). Subsequent studies utilized PEG experiments to address slope effects (e.g., Gregg & Fink, 2000). Extrapolating laboratory experiments to other terrestrial bodies such as Mars has been attempted in order to constrain eruption parameters and predict expected morphologies, although the image resolution at the time of these studies was limited to >150 m/pixel (Fink & Griffiths, 1992; Gregg & Fink, 1996; Peters, 2020). Laboratory experiments, in conjunction with rheologic modeling and remote sensing geomorphology, therefore provide an additional constraint on prehistoric eruption conditions on Mars.

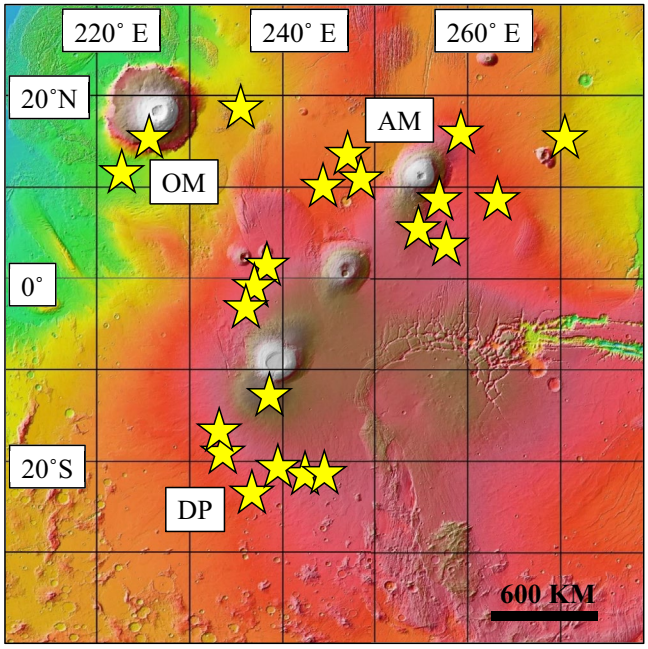

Figure 2. Map of study area, the Tharsis volcanic province. Base map is Mars Orbital Laser Altimeter colorized topography, with warm colors representing areas of higher elevation. Square label demarks Olympus Mons (OM), Ascraeus Mons (AM), and Daedalia Planum (DP).

3. Geologic Setting

3.1. Tharsis Volcanic Province

The Tharsis region represents the largest volcanic province on Mars (Figure 2), containing the tallest volcano in the solar system (Olympus Mons at ~22 km), one of the largest volcanoes on the planet in areal extent (Alba Mons at ~1.15 × 10^6 km^2), and the Tharsis Montes—three large shield volcanoes (Carr, 1973, 1974; Crumpler & Aubele, 1978; Greeley & Spudis, 1981; Plescia, 2004; Scott & Tanaka, 1981). In addition, the region contains innumerable lava flows and small shields, in what is sometimes characterized as plains-style volcanism (Baloga & Glaze, 2008; Glaze et al., 2009; Greeley, 1982; Hauber et al., 2011; Hiesinger et al., 2007). Tharsis dominates the western hemisphere of the planet and occupies a region from ~60°N to ~40°S and 210°E to 300°E and ~4,000 × 6,000 km. Volcanic activity began ~4 Ga and has occurred within the last ~100 Ma (Carr, 1973, 1974; Plescia, 2004; Scott & Tanaka, 1981; Werner, 2009). The 40 lava flows featured in this study occur throughout the Tharsis volcanic

province, primarily on and around Olympus Mons, in the volcanic plains surrounding the Tharsis Montes, and Daedalia Planum. A brief summary is given of each region.

3.1.1. Olympus Mons and Ascraeus Mons

Olympus Mons and Ascraeus Mons are two large shield volcanoes in the Tharsis volcanic province. Olympus Mons is 600 km across and 22 km high and Ascraeus Mons is 400 km across and 15 km high. Olympus Mons is situated northwest of the Tharsis Montes and southwest of Alba Mons (Figure 2), while Ascraeus Mons (located east of Olympus Mons) is the northernmost of the Tharsis Montes (Carr, 1973; Greeley & Spudis, 1981; Plescia, 2004; Werner, 2009). Both volcanoes display nested caldera complexes and evidence of widespread effusive eruptions. Extensive dust cover prohibits compositional analyses of either volcano, but both volcanoes are morphologically similar to Hawaii and the Galapagos shield volcanoes and a basaltic composition has been inferred for their erupted lavas (e.g., Bleacher, Greeley, Williams, Cave, & Neukum, 2007; Bleacher, Greeley, Williams, Werner, et al., 2007; Byrne et al., 2012; Christensen, 1986; Rogers & Christensen, 2007). Both volcanoes display gentle sloping flanks (~4–6°) with some steepening on the upper flanks (e.g., Plescia, 2004). Although construction of Olympus Mons and Ascraeus Mons is believed to have been largely completed by the Late Noachian or Early Hesperian (>3.6 Ga), their surfaces have been dated to ~100–800 Ma based on crater count modeling (e.g., Neukum et al., 2004; Werner, 2009; Xiao et al., 2012). Some of the youngest features on Olympus Mons and Ascraeus Mons include lavas on the floors of the nested calderas (~100–200 Ma), some flank lava flows (~50 Ma), and small satellite vents and arcuate graben (e.g., Byrne et al., 2012; Neukum et al., 2004; Peters & Christensen, 2017; Tanaka et al., 2014; Werner, 2009).

3.1.2. Volcanic Plains and Daedalia Planum

Volcanic plains formed by countless overlapping lava flows cover much of the terrain within the Tharsis volcanic province (Figure 2) producing a monotonous topography of gentle slopes, punctuated by low shields, cinder cones, graben, and the central volcanoes (e.g., Carr, 1973, 1974; Greeley & Spudis, 1981; Hauber et al., 2011). Individual lava flows can extend hundreds of kilometers from their sources, which include dozens of low shield volcanoes, the Tharsis Montes, and buried sources (Baloga & Glaze, 2008; Carr, 1973, 1974; Crumpler & Aubele, 1978; Glaze et al., 2009; Greeley & Spudis, 1981; Hauber et al., 2011; Hiesinger et al., 2007). Daedalia Planum—an example of this terrain—is an 18×10^6 km^2 volcanic plain on Mars located southwest of Arsia Mons, one of the Tharsis Montes (Giacomini et al., 2012; Plescia, 2004; Werner, 2009). It too hosts very long lava flows (>200 km in some cases), with many believed to be sourced by activity related to Arsia Mons, the southernmost and oldest of the Tharsis Montes (e.g., Crown & Ramsey, 2016; Giacomini et al., 2009, 2012; Plescia, 2004; Scott & Tanaka, 1981; Werner, 2009). Recent studies on Daedalia Planum have measured average lava flow thicknesses of 35–70 m using high-resolution image and elevation data, observed inflation in lava flows using possible lava rises and tumuli, and attempted compositional analysis via spectral mapping (e.g., Giacomini et al., 2009, 2012).

4. Methodology

4.1. Data Sets and Analyses Criteria

We used image data from the Mars Reconnaissance Orbiter (MRO) Context Camera (CTX: ~5 m/pixel) (Malin et al., 2007), the Mars Odyssey Thermal Emission Imaging System in the infrared (THEMIS IR: 100 m/pixel) (Christensen et al., 2004), and the MRO HiRISE (~0.25 m/pixel) instruments (McEwen et al., 2007). We utilized topographic data from the Mars Global Surveyor Mars Orbital Laser Altimeter (MOLA: ~463 m/pixel) digital elevation model (DEM) (Zuber et al., 1992) data set, as well as Mars Express High-Resolution Stereo Camera (HRSC) DEM (DEM cell size: 50–75 m) (Jaumann et al., 2007). Although high resolution HRSC DEMs did not cover the entire study area, they were more extensive than CTX and HiRISE DEMs and readily available. As a result, some flows were characterized using the MOLA DEM (e.g., Glaze et al., 2003). Due to the resolution of the MOLA DEM, larger lava flows were given priority when HRSC DEM coverage was not available. All data sets were accessed and analyzed using the Java Mission Planning and Remote Sensing GIS software (e.g., Gorelick et al., 2003).

For this study, we considered lava flows in the Tharsis volcanic province because of the large number of well-preserved flows and extensive overlapping data sets. We selected 40 lava flows based on the following criteria: (a) morphology and (b) data coverage. We prioritized flows with relatively unobstructed flow along their lengths and relatively well-defined margins. In all cases, the full extent of the original flow was not preserved due to superimposed lava flows, impact craters, or erosion/degradation. These processes reduced the available flow area for study and also resulted in the erasure of the flow source. As a result, our flow lengths, volumes, and volumetric flow rates represent minima. We also prioritized lava flows with adequate data coverage. Every selected lava flow had CTX visible image coverage and at least partial HRSC and/or complete MOLA DEM coverage. Despite the ≥1 m dust mantle that blankets the Tharsis volcanic province, lava flow surface texture is relatively well preserved and discernible (Christensen, 1986). Compression ridges are visible on a number of lava flows, owing to the resilience of these features in the face of erosion, degradation, and dust cover. However, finer scale morphologies, such as pahoehoe lava lobes (which tend to be meter-scale features), if originally present, are not visible due to extensive dust mantling that masks meter and sub-meter scale topography. Overall, the morphologies and morphometric properties of lava flows in the Tharsis volcanic province suggest a basalt to basaltic andesite composition (e.g., Bleacher, Greeley, Williams, Cave, & Neukum, 2007; Bleacher, Greeley, Williams, Werner, et al., 2007; Carr, 1974; Hiesinger et al., 2007; Hulme, 1974). We measured and calculated the length, mean width, mean thickness, surface area, volume, and mean slope for each of the 40 lava flows in this study (Table 1). The length of each flow was measured using a centerline. The mean width and thickness of each flow were calculated using multiple (i.e., ~10–60 depending on the flow length) approximately evenly spaced cross-sectional profiles. We calculated the volume by multiplying surface area by mean thickness. We applied the three models discussed above to the 40 lava flows in this study in order to estimate volumetric flow rates, bulk viscosities and yield strengths, and emplacement times. The models and how they were applied to the data set are detailed in the following section.

4.2. Models for Interpreting the Data Sets

4.2.1. Cooling-Limited and Rheologic Model

We applied a standard rheologic treatment to 34 of 40 lava flows using methods outlined by Hiesinger et al. (2007), and references therein, to calculate eruption rate and viscosity. Six of 40 lava flows were excluded because they exhibit prominent ridges likely formed through repeated overspills from a channel or tube during emplacement, in stark contrast to the typical flows for which this method was intended (e.g., Sakimoto et al., 1997). The method uses (a) the Graetz number (G_z), a dimensionless number that characterizes the ratio of the time scale of cooling by conduction at the edges or surface of the flow, to that of fluid advection downstream; and (b) Jefferey's equation, which is a steady-state momentum equation reduced to a force balance between downslope gravitational forces that drive the flow and viscous forces that impede the flow, can be expressed in terms of flow velocity, geometry, and fluid viscosity (Jeffreys, 1925; Wilson & Head, 1983). This approach requires some assumptions including: laminar flow of a Newtonian fluid; steady-state emplacement at low velocities; flow dimensions that reflect rheological properties of the flow (e.g., Hauber et al., 2011; Hiesinger et al., 2007; Wilson & Head, 1983); and a Graetz number of ~300 that defines when the flow halts, following Pinkerton and Sparks (1976).

According to a suite of observations of cooling-limited lava flows at Mt. Etna, Pinkerton and Sparks (1976) found that flows ceased advancing at G_z of approximately 300, when crust extent and strength was sufficient to prevent the continued propagation of the small amount of melt remaining in the core of the flows. Guest et al. (1987) questioned the value of 300 because Pinkerton and Sparks (1976) did not take into account branching of lava flows or the possibility of volume-limited flows. However, for cooling-limited flows, Guest et al. (1987) place the halting Graetz number at approximately 230, very close to the assumed value of 300. The Mars flows studied here exhibit limited to no branching, and given their large volumes (see below), they were unlikely to have been volume-limited. We therefore assume that they were cooling-limited and proceed with a halting Graetz number value of 300. Graetz number (G_z) can be expressed as

$$G_z = \left[Q / \left(\kappa x\right)\right]\left(w / h\right) \quad (1)$$

Table 1
Data on 40 Lava Flows in Tharsis Volcanic Province on Mars Investigated in This Study

Flow #	Lat (N)	Long (E)	Region	Length (km)	Mean width (km)	Mean flow thickness (m)	Volume (km^3)	Mean slope (degrees)	Ψ (morphology)
1	18.53	235.94	E of Olympus Mons	21	5.6	11	1.3	0.4	High (levees)
2	11.914	244.629	Tharsis	310	18	46	280	0.4	High (levees)
3	14.504	248.246	Tharsis	310	29	39	440	0.3	Very high-high (smooth-levees)
4	15.199	226.654	Olympus Mons	18	0.59	27	0.38	6.6	High-intermediate (levee-folds)
5	15.008	226.823	Olympus Mons	33	0.57	12	0.25	6.6	High-intermediate (levee-folds)
6	15.761	224.764	Olympus Mons	19	3.0	25	1.5	4.2	High (levees)
7	11.739	224.015	S of Olympus Mons	100	6.9	26	23	0.4	High (levees)
8	11.597	222.495	S of Olympus Mons	41	6.5	14	1.8	0.4	High (levees)
9	−19.332	243.262	Daedalia Planum	78	5.9	25	12	0.7	High (levees)
10	−20.945	240.957	Daedalia Planum	140	5.9	33	34	0.7	High (levees)
11	−21.733	242.555	Daedalia Planum	58	16	36	38	0.6	High-intermediate (levee-folds)
12	−23.297	242.812	Daedalia Planum	270	19	45	270	0.8	High (levees)
13	−22.547	244.16	Daedalia Planum	200	12	30	100	0.6	High (levees)
14	−23.195	237.617	Daedalia Planum	220	6.0	32	52	0.7	High (levees)
15	−19.081	234.684	Daedalia Planum	92	3.8	15	6.1	0.8	High-intermediate (levee-folds)
16	−17.307	233.48	Daedalia Planum	170	3.2	16	12	1.0	High (levees)
17	−22.665	237.6084	Daedalia Planum	106	4.5	17	10	0.6	High (levees)
18	8.945	257.408	Ascraeus Mons	16	4.1	15	0.99	0.8	Intermediate (folds)
19	15.521	261.191	Ascraeus Mons	79	4.2	23	8.3	0.9	High (levees)
20	12.102	250.046	W of Ascraeus Mons	99	12	37	65	0.5	High (levees)
21	11.193	248.41	W of Ascraeus Mons	120	17	38	73	0.5	Very high-high (smooth-levees)
22	15.757	225.213	Olympus Mons	15	1.2	18	0.33	4.6	High (levees)
23	15.814	225.379	Olympus Mons	30	5.9	91	8.2	5.4	Low (ridge)
24	15.156	225.105	Olympus Mons	27	1.3	18	0.77	4.7	High (levees)
25	14.997	225.298	Olympus Mons	60	6.8	68	14	6.7	Low (ridge)
26	16.089	227.269	Olympus Mons	13	3.7	64	1.6	4.2	Low (ridge)
27	15.91	227.239	Olympus Mons	28	2.2	37	1.1	5.5	Low (ridge)
28	15.178	259.464	Ascraeus Mons	48	4.6	31	3.4	1.2	Low (ridge)
29	15.689	259.131	Ascraeus Mons	29	7	38	3.9	1.0	Low (ridge)
30	8.572	263.609	Tharsis	44	7.1	29	9.0	0.4	High (levees)
31	−12.934	239.423	Daedalia Planum	25	2.1	31	1.7	1.4	High (levees)
32	−0.879	237.326	Tharsis	77	5.9	31	15	0.6	High (levees)
33	−3.006	239.936	Tharsis	69	6.0	29	12	0.8	High (levees)
34	16.210	261.309	Tharsis	72	3.7	25	7.13	0.6	High (levees)
35	5.018	256.914	Tharsis	99	3.1	16	5.09	0.8	High (levees)
36	5.229	254.687	Tharsis	23	1.3	11	0.46	0.7	High (levees)
37	5.371	255.546	Tharsis	38	1.9	13	1.09	0.7	High (levees)

Table 1
Continued

Flow #	Lat (N)	Long (E)	Region	Length (km)	Mean width (km)	Mean flow thickness (m)	Volume (km^3)	Mean slope (degrees)	Ψ (morphology)
38	3.576	259.678	Tharsis	128	4.9	18.1	11.91	0.5	High (levees)
39	1.347	238.558	Tharsis	71	6.7	23	12.03	0.5	High (levees)
40	15.51	271.857	Tharsis	220	14	55	173.69	0.6	High (levees)

where Q is the effusion rate, κ is thermal diffusivity of the lava, which is a function of its composition ($m^2\ s^{-1}$), x is flow length, w is mean flow width (Table 1), and h is mean flow thickness (Table 1) (Wilson & Head, 1983). This equation is a modification of the original Graetz number for cooling of a fluid in a cylindrical pipe. Equation 1 accounts for the fact that thinner flows cool faster than deeper flows by including the aspect ratio w/h (Hulme & Fielder, 1977). Here effusion rate, Q, was obtained by rearranging Equation 1, assuming a halting Graetz number of 300, using the flow geometries measured from the previously described data sets (Table 1), and applying the thermal diffusivity of basalt, 5.00×10^{-7} m^2/s (e.g., Hon et al., 1994; Pasckert et al., 2012; Wilson & Head, 1983).

Jeffrey's equation can be used to relate the effusion rate of a flow to its viscosity, density, and flow dimensions. It is derived for flow on an infinitely wide plane and is written as follows for broad flows (Jeffreys, 1925).

$$\eta = \rho g h^3 w \sin \alpha \ / \ 3Q \tag{2}$$

where η is the effective dynamic viscosity of the flow during emplacement and propagation, ρ is the lava density during emplacement, w and h are the flow dimensions as described previously, Q is volumetric effusion rate, α is the underlying slope, and 3 is a constant used for flows that are much wider than they are deep (Jeffreys, 1925). We assumed a density of 2,700 kg/m^3 which is consistent with estimates from previous studies and within the range of terrestrial basalt values (e.g., Hauber et al., 2011; Hiesinger et al., 2007; Pasckert et al., 2012; Rowland et al., 2004). Q from Equation 1, along with flow geometry, underlying slope, and magma density were used in Equation 2 to calculate dynamic viscosity η. Emplacement times were estimated from Q and measured individual flow volumes.

4.2.2. Laboratory Experiments and Ψ

We classified each of the 40 observed lava flows by dominant surface morphology, which corresponds to a particular Ψ regime (Fink & Griffiths, 1990; Gregg & Fink, 1996). Ψ is a powerful way of understanding the dynamics of flow emplacement using only flow morphology. Because it is a dimensionless parameter, Ψ can be applied to flows of any composition, rheology, and scale so long as reasonable emplacement constraints such as ambient conditions and properties of the flowing liquid can be assumed. Five flow morphologies corresponding to discreet Ψ ranges have been observed. Those morphologies from high to low, $\Psi > 55$ to $\Psi \sim 1$, are: No Crust, Levees, Folds, Rifts, and Pillows (Figure 1) (Fink & Griffiths, 1990, 1992; Gregg & Fink, 2000). Transitional morphologies are also observed in the lab and on Mars, demonstrating that the morphologies are produced on a continuum. And, as stated previously, the textures observed in the laboratory are observed in nature—from terrestrial felsic lava flows to sulfur flows (e.g., Fink et al., 1983; Gregg & Fink, 1996; Griffiths & Fink, 1992; Peters, 2020; Pieri et al., 1984).

In the analysis presented, we assumed that the predominant morphology observed represents the dominant Ψ regime during the time of emplacement (Figure 1). The validity of this assumption has been demonstrated in the laboratory to the extent possible (Fink & Griffiths, 1990, 1992; Gregg & Fink, 2000). Although there exists the possibility that flows pass through a number of morphological regimes throughout the emplacement process, the final morphology preserved in the rock record is the only source of data we have for the surface of Mars. We proceed with this caveat in mind, and thus assume that our calculations based on Ψ regime best represent the dominant flow emplacement conditions. Furthermore, each flow was assigned a Ψ value range corresponding to the observed morphology. Some transitional morphologies (e.g., levee-fold) were observed, while no pillow morphologies were definitively observed. We classified the lava ridges, previously observed on Olympus Mons, Alba Mons, and other localities, and interpreted as lava tubes (Bleacher, Greeley, Williams, Cave, & Neukum, 2007; Bleacher, Greeley, Williams, Werner, et al., 2007; Sakimoto

et al., 1997), under the rift morphology, which represent lower values of Ψ. Our interpretation is based on laboratory analog experiments using PEG wax performed on slopes, which yielded ridge-like structures produced by lava tubes that advanced downslope piecemeal, with the "rifting" describing fracturing in the surface crust (Peters, 2020).

Ψ can be written in terms of a modified Peclet number, Π, a nondimensional cooling timescale for the crust, τ_s, and a ratio of temperature differences including ambient, solidification, and wax or lava temperatures, θ_s (Fink & Griffiths, 1990, Equation 10, provided here as Equation 3).

$$\Psi = \Pi \tau_s \left(\theta_s\right) \tag{3}$$

Π incorporates the traditional Peclet number (Pe), which is the ratio of the rate of advective heat transport by the flowing lava to the rate of conductive heat transport at the flows surface. Π also includes the effects of reduced gravity (g'), kinematic viscosity (ν), thermal diffusivity of the wax or lava (κ), and the timescale (λ) over which the contact temperature of the wax or lava reaches the temperature of the ambient environment far from the lava surface, where the contact temperature is defined as the temperature at the interface between wax or lava and the ambient.

$$\Pi = \left(\frac{g'}{\nu}\right)^{\frac{2}{3}} \kappa^{\frac{1}{3}} \lambda Pe^{\frac{1}{3}} \tag{4}$$

Like Pe, Π represents a ratio of a characteristic advective flux or flow rate downstream to a characteristic thermal diffusion rate at the surface of the flow (Fink & Griffiths, 1990).

Ψ can also be written as a ratio of the solidification and advection time scales, which is more descriptive.

$$\Psi = \frac{t_s}{t_a} \tag{5}$$

Here, t_s represents the timescale of solidification of the surface crust and t_a represents the timescale of horizontal advection. Using the relationships in Equations 3 and 4, we can calculate a range of effusion rates corresponding to the Ψ ranges for each flow morphology, for assumed Mars eruption and ambient conditions. From those effusion rates and measured flow volumes, we can also calculate a range of emplacement times for each flow.

However, in order to translate the Ψ ranges to eruption rates, we are required to make simplifying assumptions about the ambient environment and the erupted liquid. In the lab, the ambient environment corresponds to the chilled bath or a sucrose solution and the erupted fluid refers to the PEG wax. For Mars, these values correspond to the ambient environment of the Martian surface and the lava flow. We assumed that radiation is the primary way a lava flow loses heat on Mars based on previous work, which found that radiative heat fluxes on Mars dominate in comparison to convective heat flux on Earth during the initial cooling of a flow (e.g., Danes, 1972; Gregg & Fink, 1996; Griffiths & Fink, 1992; Rowland et al., 2004). As a result, convective and conductive losses are considered to be negligible. In addition to the flow properties mentioned previously (i.e., density, thermal diffusivity), we assumed an ambient environment temperature of 180 K, an atmospheric density of 0.02 kg/m^3, a solidification temperature of 900°C, and gravity of 3.71 m^3/s (e.g., Peck, 1978; Rowland et al., 2004). The ambient environment temperature, atmospheric density, and gravity represent the average values for Mars (e.g., Rowland et al., 2004) and deviations of these values do not significantly impact our results. For values related to the Martian atmosphere, specifically kinematic viscosity, we assumed pure CO_2 (Chemical Rubber Company, 1984; Crane Company, 1988). The basalt solidus is cited as 980°C; however, the internal temperature of barely mobile basalt flows has been measured at temperatures as low as 800°C and basalt flows on Mt Etna have been typically modeled with solidification temperatures of ~870°C (Belousov et al., 2015; Peck, 1978; Pinkerton et al., 2002; Vicari et al., 2007). We find a value of 900°C to be reasonable and within the range of previous studies. We assumed the lava flows in our study erupted at 1150°C, which is similar to the erupted temperature of basalts at Hawaiian volcanoes and Mt. Etna and within the range of typical terrestrial basalts (1100–1250°C, Danes, 1972; Harris & Rowland, 2001, 2015; Pinkerton, 1987; Vicari et al., 2007).

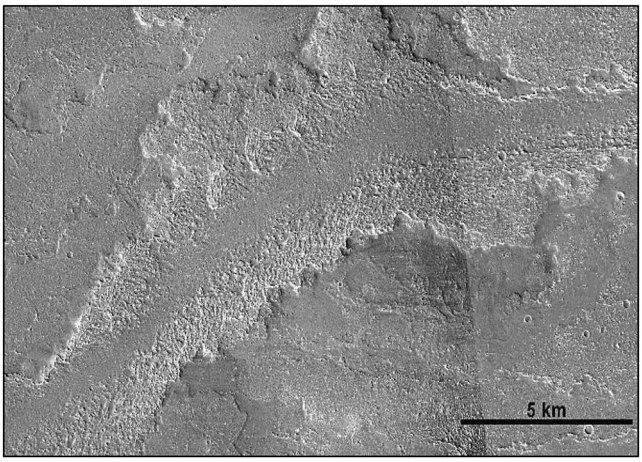

Figure 3. CTX image of a long, self-replicating lava flow in the volcanic plains of Tharsis south of Olympus Mons. The channel is clearly defined, has an approximately constant width, and levees are well developed and near constant width.

4.2.3. Self-Replicating Lava Flow Model

Many of the lava flows observed in the major Martian volcanic provinces of Tharsis and Elysium display a similar repetitive morphology. Baloga and Glaze (2008) termed these flows "self-replicating lava flows" and identified a set of defining criteria: morphologic characteristics that repeat over the length of the flow, relatively constant channel and levee dimensions, and a single channel that is visible for most of its length (Figure 3). Their corresponding model of propagation takes into account mass removed from the active molten lava flow during the formation of lateral levees at the flow front as it propagates. The model assumes that levees are created at the flow front due to a vertical parabolic velocity profile in the molten core consisting of a Newtonian fluid, in which fluid at the top of the flow is traveling downslope faster than fluid at its base (Figure 4) (Baloga & Glaze, 2008; Glaze & Baloga, 2006). The total excess flow rate (Q_{ex}) that forms the levees is calculated as a product of the average excess flow velocity (u_c), width of the channel, and the thickness of the nondeformable crust atop the flow (Baloga & Glaze, 2008, Equation 6). The excess mass is then left behind as the flow front advances at

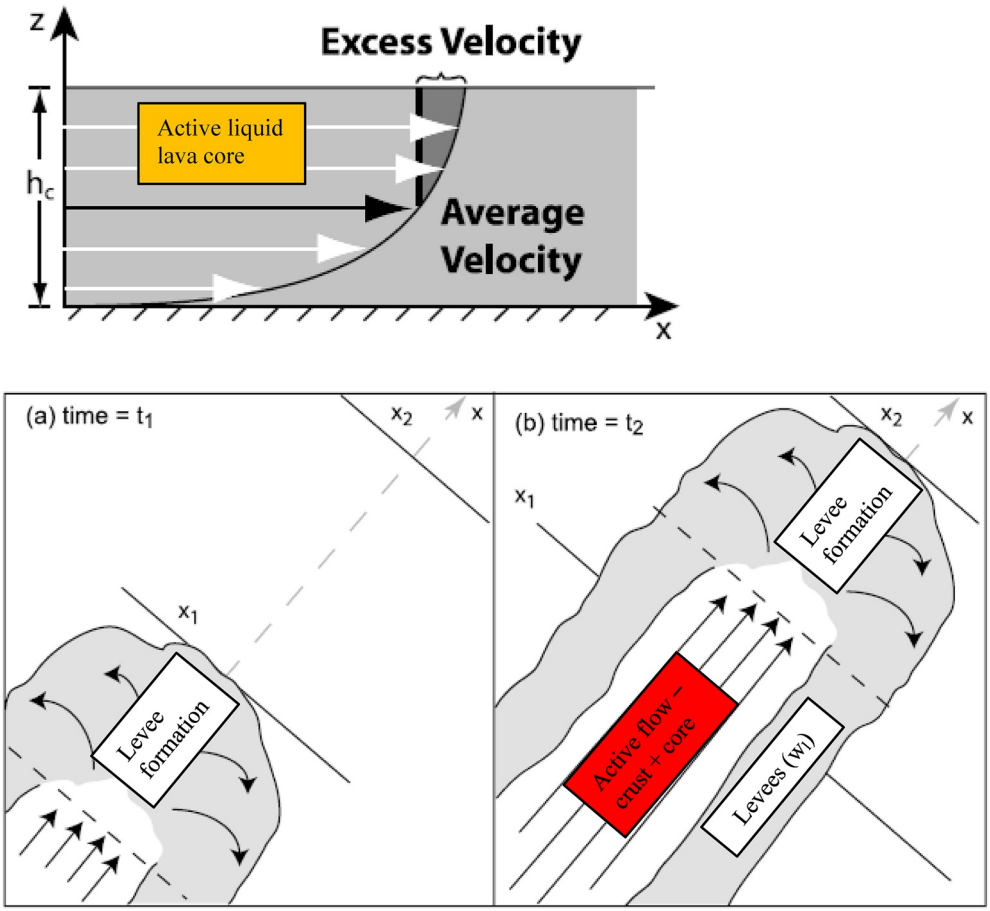

Figure 4. Modified from Baloga and Glaze (2008) illustrating how "self-replicating" lava flows, which include well-defined channels and levees of relative constant width, are produced. As the flow passes a given point, some mass of the flow at the flow front is deposited to form levees.

the average downstream velocity of the molten core (u_c). Only a subset of lava flows in this study—13 of 40—met the Baloga and Glaze (2008) criteria of self-replicating flows.

Using methods outlined in Baloga and Glaze (2008) and references therein, we calculated eruption rates (Q) and the resultant viscosities and emplacement times for the 13 qualifying lava flows across the Tharsis volcanic province. To do so, we first calculated the levee widths (w_l):

$$w_l = \frac{Q_{ex}}{u_c \times h_l} \tag{6}$$

$$= \frac{w_c}{h_l}\left[\frac{h_c}{3\sqrt{3}} + \frac{1}{2}\left(h_l - h_c\right)\right]$$

where h_l is the levee thickness. Equation 6 assumes that the excess volume flux Q_{ex} is u_c times the dimensions of the levees, h_l and w_l. The crust thickness is assumed to be the difference between total flow thickness and the liquid core thickness (h_c). The total flow thickness is approximated by the height of the levees, such that the crust thickness is h_l–h_c. Crust thickness was found as a function of distance downstream and the data was smoothed as in Baloga and Glaze (2008) reaching an asymptotic value (Figure 8). A cooling time for the asymptotic crust thickness to form was calculated using solidification by conductive cooling modified from Hon et al. (1994). The emplacement duration of the flow was assumed to be the same as the time required for crustal growth. Average effusion rate was calculated for each flow using its total volume and the emplacement time.

4.2.4. Yield Strength Calculation

Our use of Equations 1 and 2 above assume Newtonian behavior, allowing viscosity to be calculated from Jeffrey's equation (Equation 2). However, many suggest that most lavas, especially those cooling during emplacement, behave as Bingham fluids (e.g., Moore et al., 1978). In order to explore this rheology further, we estimate the yield strength (σ) of each flow using underlying slope (α), flow thickness (h), and an assumed lava density of 2,700 kg m^{-3} (following the procedure of Hiesinger et al., 2007 and references therein).

$$\sigma = \rho g \sin\left(\alpha\right) h \tag{7}$$

5. Comparison of Applied Models and Sources of Uncertainty

All of the models used in this study make simplifying assumptions about the rheology, dynamics, and emplacement of the lava flow along with the conditions of the ambient environment. These simplifying assumptions result in uncertainties. However, a more complex model, even with simplifying assumptions such as the self-replication model, produces results closer to replicating real world processes. The purpose of studying Martian lava flows with multiple methods is an attempt to offset some of the uncertainties and converge on a more accurate picture of the eruptive conditions that produced these impressive flows. While certain aspects of more than one of the models are rooted in similar origins—such as Jefferey's equation—newer models have become more complex in an attempt to better understand the complicated conditions in nature. Here we will discuss the simplifying assumptions of each model, what they mean for real lava flows, and how they affect our results.

5.1. Rheology Models (Jeffrey's Equation, Graetz Number, and Self-Replication Model)

Using the dimensions of an emplaced flow to calculate its effusion rate overestimates the effusion rate of the lava flow by assuming that the entire flow is active during the time of emplacement (e.g., Baloga & Glaze, 2008; Glaze et al., 2009; Hauber et al., 2011; Hiesinger et al., 2007). We know from observations of active lava flows that the entire width of the lava flow is rarely active at the time of emplacement in fact, most of the flow is relatively immobile with mass stored in immobile levees (e.g., Baloga & Glaze, 2008; Baloga et al., 1998; Glaze et al., 2009). The height of the flow is also misleading because the height of a solidified, emplaced flow may not characterize the true height of the flow during emplacement (e.g., Baloga & Glaze, 2008; Baloga et al., 1998; Glaze et al., 2009). For example, many flows on Mars display prominent levees and the highest point of these levees is often assumed to represent the height of the flow at the time

of emplacement. That height likely represents a maximum of some interval of time that does not represent conditions during the majority of time when the flow was active. Taken together, when calculating effusion rate from the Graetz number, this equation can overestimate eruption rates, sometimes by more than an order of magnitude. Erroneously high eruption rates would imply exotic lava compositions and/or very large subsurface pathways through the Martian crust. The Graetz number also represents an approximation of flow cessation. Varying the Graetz number affects calculated effusion rates and ultimately the calculated viscosity. We varied the Graetz number by ±70. A Graetz number of 230 decreases the calculated eruption rate by ∼23% and increases viscosity by ∼30%, while a Graetz number of 370 increases calculated eruption rate by ∼23% and decreases viscosity by ∼19%.

Jeffrey's equation—originally developed to calculate the flow of water in a rectangular, inclined channel—assumes that the flowing fluid has a Newtonian rheology, like water (Jeffreys, 1925; Nichols, 1939). Although the superheated interior of lava flows, especially flows confined in tubes and channels, behave as Newtonian fluids, lava is better, though not perfectly, approximated by a Bingham rheology and recent studies have shown it is best approximated by a power law relationship due to crystallization and interaction between the crust and liquid core (e.g., Bruno et al., 1996; Hulme, 1974). However, different portions of the flow can behave as a Newtonian, Bingham, or power law rheology (Bruno et al., 1996). Due to the overestimate of the effusion rate, Jeffrey's equation will produce an answer that underestimates the lava flow's viscosity. As lava flows cool and develop a crust, the viscosity and rheology of the flow changes (e.g., Fink & Griffiths, 1990; Hallsworth et al., 1987). Thus, portions of the lava flow farther from the heated interior—such as the margins of the channel or the levees—will not have a Newtonian rheology despite possibly remaining malleable (Bruno et al., 1996). There is an added complication that Jeffrey's equation assumes that the density and viscosity of the flow remains effectively constant for the entirety of the flow. In reality, the density and viscosity of a lava flow begins changing the moment it erupts and continues to change until the flow ceases to flow. The density and viscosity are lowest near the vent because the flow is hotter, while they are highest at the end of the flow where it is cooler and has undergone crystallization (e.g., Crisp & Baloga, 1994). We chose a density of 2,700 kg/m^3 which falls in the range of basalts 2,600–3,200 kg/m^3 and is not dissimilar for values used in previous studies (e.g., Hiesinger et al., 2007; Pasckert et al., 2012; Rowland et al., 2004). If our densities are in error, they will affect the calculated viscosities and yield strengths proportionally. For example, if we assume a density of 2,000 kg/m^3, the calculated viscosity and yield strength decreases by ∼26%.

Key contributors to uncertainty in the self-replication model are the measured flow length, the thickness of the flow, and the assumed density. Since the measured flow lengths are likely absolute minima, we have underestimated the flow area and volumes. If we assume our flow lengths are in error by 25% (i.e., the flows are 25% longer than measured), then our eruption rates and viscosities would be in error by ∼20%. A 25% longer flow length would also decrease calculated viscosity by ∼20%. Although measuring an accurate flow length is important, the level of uncertainty here does not significantly impact our results or their implications.

Variability in the density has the largest impact on calculated yield strength. If the assumed density is 50% lower than expected, our calculated yield strengths decreased by ∼50%. We do not expect our densities to vary by such a large amount. A 25% decrease in density results in a ∼26% decrease in calculated yield strength. The latter case does not significantly impact our results.

Flow thickness impacts calculated viscosity, specifically our estimates of the core thickness (i.e., the fluid core of the lava flow beneath the surface crust). If core thicknesses were 25% lower than calculated, then calculated viscosities decrease by 44%. If core thickness is 25% greater than expected, the calculated viscosities increase by 57%. As core thickness is extrapolated from observed data, smoothed using a polynomial fit, and relies on underlying assumptions about crust solidification and thickness, it is perhaps the largest source of error in this model. That said, for most of our flows, a 25% error in the estimated core thickness does not change the calculated viscosity by an order of magnitude.

5.2. Laboratory Analog Experiments and Ψ

The utilization of Ψ provides a powerful way of investigating a lava flow by using its morphology to determine the flow conditions at the time of emplacement. The applicability of laboratory analog experiments to

terrestrial environments has been a goal for decades and provides a way to investigate the complexity inherent within lava flow emplacement. In order to calculate eruption rates and the resultant emplacement times from Ψ, simplifying assumptions regarding lava flow and ambient condition properties are required. For the lava flow, density, kinematic viscosity, solidification temperature, eruption temperature, emissivity, thermal diffusivity, heat capacity, water content (implicit), vesiculation (implicit), crystal content (implicit), and final flow morphology are required. Assumptions about the ambient conditions include density, kinematic viscosity, thermal diffusivity, thermal expansion, heat capacity, and temperature. Because we are interested in lava flows on Mars, we are assuming a basalt to basaltic andesite composition. This is consistent with the flow morphology and the observations of a variety of studies aimed at volcanism and the Martian crust (e.g., Baloga & Glaze, 2008; Carr, 1973, 1974; Glaze et al., 2009; Hauber et al., 2011; Hiesinger et al., 2007; Hulme, 1974; Rogers & Christensen, 2007).

Some of the input variables into Ψ for lava flows have been measured for various lava flows in the field and can be estimated with some confidence. Thermal diffusivity and heat capacity are well constrained for basaltic lava flows. Emissivity, impacted by the fraction of surface crust present on a lava flow, has also been studied both observationally and theoretically for lava flows and we find our estimate of 0.9 is consistent with the literature (e.g., Cashman et al., 2006; Rowland et al., 2004; Vicari et al., 2007). Because Ψ is rooted in laboratory analog experiments performed with a substance, which does not mimic vesiculation, there is an implicit assumption that water content, vesiculation, and crystal content have a negligible impact on the morphology of the lava flow. As lava flows propagate away from the vent, the exsolution of water from the molten lava increases the viscosity. However, terrestrial basalts tend to be drier than other more felsic compositions with ∼2 wt. % water and Martian basalts are thought to be particularly dry with estimates of <1.5 wt. % water (e.g., Black & Manga, 2016). On the other hand, crystallization increases with increasing distance from the vent as the flow cools which increases the flows viscosity by orders of magnitude along its length (e.g., Crisp & Baloga, 1994). Although these variables work to retard the advancement of a lava flow, they do not tend to impact the overall morphology of a flow and primarily impact the distal portion of the flow and the final length of the flow, especially for basalts. Martian lava flows have been observed to preserve a dominant morphology, just like flows on Earth, that reflects other more dominant factors such as effusion rate and crust formation than increases in viscosity along its length. Unlike the other models used in this study, Ψ does not output a dynamic viscosity. For Ψ, kinematic viscosity is an input because the dynamic viscosity of the analogous material (PEG 600) can be measured. As a result, when applying this model to actual lava flows, the viscosity must be measured, calculated, or assumed. The input kinematic viscosity (dynamic viscosity divided by density) is that of the liquid at the moment of eruption. We chose a value of 270 Pa s at 1150°C. For basaltic lava (and potentially more mafic compositions), a dynamic viscosity of $\sim 10^2$ at the moment of eruption is reasonable. In Hawaii, recently erupted basalt can have viscosities of $\sim 10^2$–10^3 Pa s, similar to Mt. Etna ($\sim 10^3$) (e.g., Harris & Rowland, 2015; Self et al., 2008). Increasing the dynamic viscosity at the vent by one order of magnitude to 2,700 Pa s, increases the calculated eruption rates by four orders of magnitude. The resultant values become unrealistic.

The density, solidification temperature, and eruption temperature of lava flows is much harder to constrain on Mars. On Earth, a range of values for these variables has been observed across lava flows of basaltic composition. Although Martian meteorites and relatively dust-free areas of the planet's surface have provided information on the geochemistry of the Martian crust, we do not have any samples of Martian lava flows and active eruptions are nonexistent. However, we assume that basalts on Earth and Mars—by virtue of their mineralogic composition—will adhere to similar ranges for density, solidification temperature, and eruption temperature. Our density value of 2,700 kg/m^3 falls near the boundary of basalts (2,700–3,200 kg/m^3) and basaltic andesites (2,500–2,700 kg/m^3) and is consistent with values used in previous studies (e.g., Baloga & Glaze, 2008; Hauber et al., 2011; Hiesinger et al., 2007; Pasckert et al., 2012; Rowland et al., 2004). If we decrease the input density by 25% (∼2,000 kg/m^3), the calculated eruption rates increase by one order of magnitude. Decreasing it further (by 50%) to 1,350 kg/m^3, the calculated eruption rates increase by two orders of magnitude. Thus, constraining the density to a reasonable value is important. We find it unlikely that basalts—and possibly more mafic compositions for some flows—erupted at densities lower than 25% below our input values, especially if ascending Martian magmas are believed to exsolve volatiles at greater depths (e.g., Wilson & Head, 1983). Thus, we believe that a value of 2,700 kg/m^3 is reasonable.

Basalts solidify over a range of temperatures (800–1100°C) due to assemblage of minerals, which solidify at different temperatures. Previous studies have used a variety of values for the solidification temperature, including the glass transition temperature (737°C) (Hon et al., 1994). Ψ is extremely sensitive to temperature so inputting the best approximation is crucial to obtaining a good value. Varying the solidification temperature by ±50°C changes the output of effusion rates by 1–2 order of magnitude. Using the glass transition temperature as the solidification temperature is unreasonable for our application. For starters, most basalt flows have already ceased to flow by the time they drop to ~737°C even if the interior of the flow remains relatively warm (e.g., Belousov et al., 2015). The outer crust experiences brittle deformation as the temperature drops from 1070°C to 800°C (e.g., Hon et al., 1994). This is not the same as solidification of the melt, but it can have a similar effect of ceasing flow motion. Solidification temperatures of 850–1000°C are more consistent with field observations and have been used in other studies (e.g., Belousov et al., 2015; Rowland et al., 2004; Vicari et al., 2007). A value of 900°C is close to values which have been cited as the solidification temperature of basalt—or rather, the temperature at which flow motion tends to cease for basalts. The eruption temperature must also be estimated. Basalts erupt between 1100 and 1250°C. We selected a value of 1150°C, not atypical for Hawaiian basalts. Varying the eruption rate ±50°C typically changes the calculated effusion rates by $a \leq 1$ order of magnitude. The difference in eruption rates as a function of temperature is a function of the ability of a hotter flow at a lower flow rate to produce the same Ψ morphology as a cooler flow at a higher flow rate. This is due to the competing forces of heat transport through the surface versus advection of heat described by Ψ. Nevertheless, the solidification temperature chosen for Martian lava flows was applied to terrestrial flows to see if the eruption temperature range yielded effusion rates observed in nature. For example, assuming a solidification temperature at Martian conditions of 900°C, an eruption temperature of 1150°C, and a density of 2,700 kg/m^3, a channelized flow (high Ψ regime) with limited crust cover would erupt at 1,400–9,600 m^3/s. That same flow, erupted under terrestrial conditions (273 K) would erupt at 17–115 m^3/s. Both estimated ranges are reasonable and have been observed in terrestrial flows in nature at similar temperatures, albeit the Mars range would include some of the highest eruption rates observed on Earth (e.g., Walker, 1973).

Ambient conditions—while easily controlled for in the lab—must be approximated for Mars. The variables to be considered are atmospheric density, kinematic viscosity, thermal diffusivity, thermal expansion, heat capacity, and temperature. Of these variables, density and temperature are the easiest to estimate given the suite of instruments in orbit and on the surface of Mars. Thus, our values for density and temperature are backed by considerable data collection (e.g., Christensen et al., 2004). We selected an ambient Mars surface temperature of 180 K (−93°C) for Tharsis, which is reasonable given its higher elevation and consistent with THEMIS observations. Increasing the ambient temperature by 30°C reduces the calculated effusion rates by 17%–30%, whereas decreasing the ambient temperature by 30°C increased the calculated effusion rates by 27%–33%. Regardless, these changes do not significantly alter the results and implications of our study. Varying the atmospheric density by up to two orders of magnitude changed our results by only ~1%. However, due to a limited understanding of the dynamics and properties of the Martian atmosphere and uncertainty about the properties of the atmosphere at the time of lava flow emplacement, the kinematic viscosity, thermal diffusivity, thermal expansion, and heat capacity are less certain. We pulled our used values primarily from value tables and websites that approximate the Martian atmosphere as 100% CO_2 (the Martian atmosphere is 96% CO_2) and treat it as an ideal gas (e.g., Crane Company, 1988; CRC, 1984; NASA Mars Fact Sheet, 2020). These values, and their small magnitudes, do not majorly impact Ψ.

Another simplification inherent in Ψ is the application of a single dimensionless parameter to describe a single lava flow, which is inherently complex and evolving during its emplacement (e.g., Gregg & Keszthelyi, 2004). In fact, Ψ can vary depending on scale. For example, at the macroscale (kilometers), a channelized lava flow has a high Ψ, but at the meter-scale the same flow may have a low Ψ, especially near the flow margins where flow rate is low and cooling is more rapid. As a result, it is important to treat Ψ as a range of values assigned to a flow that characterize its average behavior. Because a single value cannot be assigned to a natural flow (unless all variables are known at the level of a laboratory experiment), the Ψ morphology of a flow is assumed to have been possible over a range of values. An added complexity lies in the fact that Ψ morphologies occur on a continuum, which can make introduced uncertainty when assigning Ψ ranges to flows with transitional morphologies. However, laboratory experiments and natural observations show that a dominant morphology is usually produced when a wax or lava flow is erupted and that dominant morphology reflects the general eruptive conditions and can be used to assign a Ψ regime to

the flow. Localized changes in morphology may occur due to reduced flow rates, increased viscosity, and so on and can result in a lower local Ψ, but these conditions are usually on a scale smaller than the entirety of the flow. On Mars, the vast majority of the observed lava flows exhibit a dominant morphology over most of their lengths. A few lava flows displaying transitional morphologies were observed as well, but were easily identifiable as displaying more than one Ψ regime.

6. Results

6.1. Classification of Qualitative Flow Morphologies

6.1.1. Channelized Flows—High Ψ

Channelized lava flows—a common feature of either high-volume eruptions or flows emplaced on steep slopes—are widely observed on the plains and shield volcanos of the Tharsis volcanic province (e.g., Baloga & Glaze, 2008; Carr, 1973, 1974; Greeley & Spudis, 1981). These flows are characterized by clearly defined (usually wide) channels and prominent levees (Figure 5a). The sources of these flows are obscured by the superposition of later flows and the termination of the flow is marked by a reduction of channel visibility and the fanning out of the flow into a smooth, featureless flow surface. Of the 40 lava flows in this study, 27 are considered channelized flows. Thirteen of these flows display the self-replicating morphology described in Baloga and Glaze (2008). Channelized lava flows tend to be smaller in length and width on central volcanoes than in the volcanic plains, and generally appear to correspond to the high Ψ regime and, in the lab, are produced on slopes >5° or on shallower slopes at high eruption rates (Gregg & Fink, 2000; Peiterson & Crown, 1999; Peters, 2020).

6.1.2. Corrugated (Folded) Flows—Intermediate Ψ

Corrugated flows—which are analogous to the fold morphology observed in PEG wax experiments performed in the laboratory—are a variation of channelized flows (Fink & Griffiths, 1990, 1992; Gregg & Fink, 2000). Typically, these flows display a broad, open channel and clearly defined levees. However, the inside of the channel and terminus of the flow is characterized by a corrugated surface texture (Figure 5b), interpreted to be the physical manifestation of compression ridges on the surface crust. This texture has also been observed on submarine and subaerial terrestrial flows. Keszthelyi et al. (2004) argued lava flows erupted during the Laki eruption 1783–1784 that display a corrugated texture have surfaces of rubbly pahoehoe and are evidence of unsteady eruption conditions. In this study, these flows are observed on Olympus Mons and in the volcanic plains surrounding Ascraeus Mons. Of the 40 lava flows observed in this study, five display this morphology. Of those five, four display a transitional morphology between channelized and corrugated flows. The same behavior has been observed in the laboratory and, in those cases, intermediate Ψ value ranges corresponding to transitional morphologies were assigned (Fink & Griffiths, 1990, 1992; Gregg & Fink, 2000). This is consistent with the observations by Keszthelyi et al. (2004), which if assuming the surface texture of these flows implies unsteady eruption conditions, would imply a lower mean Ψ than channelized flows not displaying a corrugated texture.

6.1.3. Smooth Flows—Very High or Low Ψ Morphology

Many lava flows on Mars display a smooth, featureless texture that some believe represent sheet flows emplaced by high eruption rates and/or low viscosity lavas, although some of these flows might instead represent inflated pahoehoe flows (e.g., Bleacher et al., 2017; Hon et al., 1994). In our study, we avoided entirely smooth lava flows due to an inability to distinguish between those flows which might represent wholesale emplacement at high eruption rates and those which might have been emplaced as pahoehoe flow fields that have undergone inflation. Nonetheless, two of the flows in our study, found in the volcanic plains, display smooth textures along certain lengths of the flow. In these instances, a long-channelized portion of the flow is also observed, and we therefore interpret these flows as transitional between channelized and sheet flows corresponding to high/very high Ψ values.

6.1.4. Lava Ridge Flows—Low Ψ on Slopes

Lava ridges have been observed on and around central volcanoes, specifically Olympus Mons and in the apron associated with Ascraeus Mons (e.g., Bleacher, Greeley, Williams, Cave, & Neukum, 2007; Bleach-

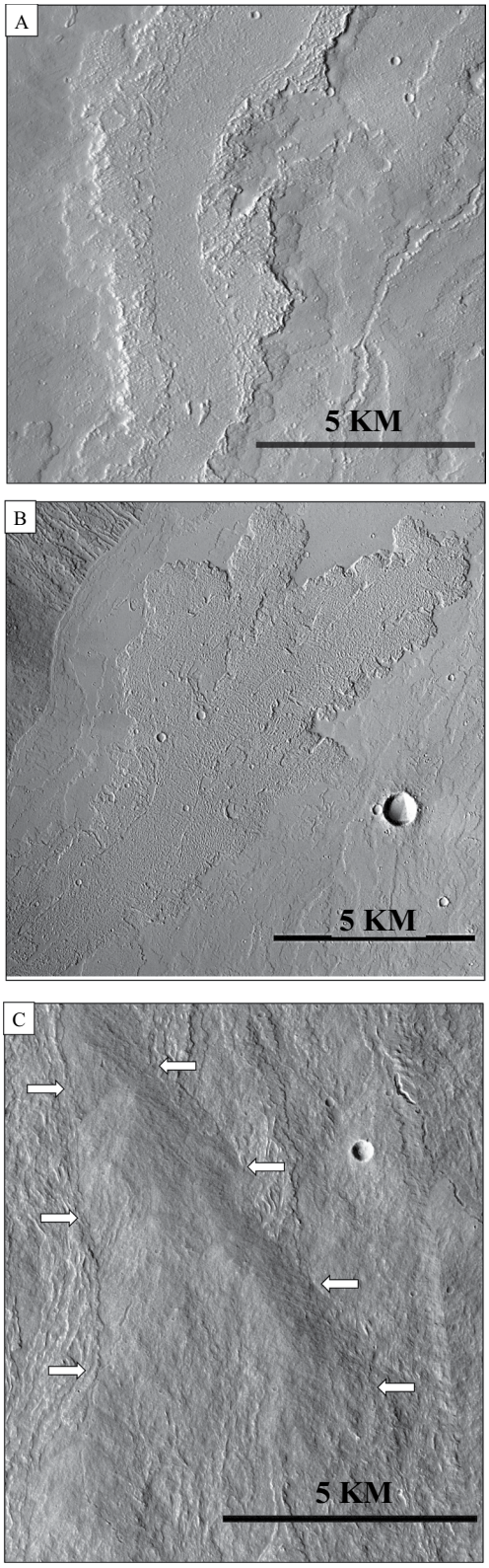

Figure 5. Examples of the three predominant flow morphologies observed in this study. All images are CTX. (a) Channelized flow (b) corrugated flow (c) ridge flow, denoted by white arrows. North is up in all images. The channelized flow has likely experienced drain out leaving behind a relatively smooth inner channel and raised levees. The ridge flow is likely a channelized flow that has roofed over—a tube-fed flow. Ridge flows are observed on Olympus Mons, Ascraeus Mons, and Alba Mons (Bleacher, Greeley, Williams, Cave, & Neukum, 2007; Bleacher, Greeley, Williams, Werner, et al., 2007; Sakimoto et al., 1997).

er, Greeley, Williams, Werner, et al., 2007; Sakimoto et al., 1997). These features have been interpreted as tube-fed flows, or lava tubes. Lava ridges generally produce a broad triangular shaped rise in cross-section. Skylights are observed on some of the ridges, where portions of the roof have collapsed into the void space below. We interpret the tube-fed flows as being associated with low Ψ values, since analogous features have been reproduced in the lab on a slope at low Ψ values. Six of the 40 studied flows are classified as lava ridges.

6.2. Flow Geometries

We measured the dimensions—length, width, and thickness—of 40 lava flows in the Tharsis volcanic province on Mars. Using these flow dimensions, we calculated flow volumes. Flows occurred in three subregions: on central volcanoes (i.e., Olympus Mons and Ascraeus Mons apron), in close proximity to central volcanoes (i.e., Olympus Mons and Ascraeus Mons), and in the volcanic plains of Tharsis. The 40 lava flows ranged in length from ~15 to 314 km. The longest flows occurred in the volcanic plains. Mean flow widths ranged from ~0.5 to 29 km, with the narrowest flows occurring on Olympus Mons. Flow thicknesses ranged from ~11 to 91 m. Flow areas and volumes ranged from ~14 to 11,000 km^2 and ~1 to 440 km^3, respectively (Figure 6). The smallest flows in areal extent and volume are observed on Olympus Mons and Ascraeus Mons apron, while the largest flows occur in the volcanic plains of Tharsis surrounding the Tharsis Montes and Daedalia Planum. The lava flows were emplaced on slopes ~0.3–6.6°, with the steepest slopes occurring on the flanks of Olympus Mons. Slopes in the volcanic plains typically ranged from ~0.3 to 1°.

6.3. Rheological Analyses

The methods described above in 4.2.1 were applied to 34 of 40 lava flows. Resulting volumetric flow rates or effusion rates ranged from 3×10^2 to $\sim 3.5 \times 10^4$ m^3/s (Table 2). Higher effusion rates were estimated for the intermontane volcanic plains and Daedalia Planum, while lower effusion rates were estimated for flows associated with Olympus Mons and to a lesser extent Ascraeus Mons. We calculated effective flow viscosities of $\sim 10^4$–10^7 Pa s and yield strengths of ~800–3×10^4 Pa. Viscosities and yield strengths were highest for flows observed on Olympus Mons and lowest for those in the volcanic plains. Modeled emplacement times for the lava flows ranged from 9 days to ~1 year.

6.4. Application of Ψ

We used assigned Ψ values to calculate eruption rates and emplacement times for all 40 lava flows. Assuming a solidification temperature of 900°C and an eruption temperature of 1150°C, calculated effusion rates using Equations 3 and 4 ranged from 0.3 to 18,000 m^3/s (Table 3). Effusion rates corresponding to each morphology are: smooth-levee flows (~12,000–18,000 m^3/s); levee flows (1,800–12,000 m^3/s); levee-fold flows (1,100–1,800 m^3/s); folded flows (65–1,100 m^3/s); rift, or tube-fed, flows (0.3–40 m^3/s). The dynamic viscosity was an input instead of an output in this model, and we used a value of 270 Pa s at an assumed density of 2,700 kg/m^3 (Hon et al., 1994; Nichols, 1939). Yield strengths are not an output of Ψ and were not calculated via this method. Emplacement times range from ~8 h to 1,500 years. The largest emplacement times (120–1,500 years) were exclusively for the lava ridge flows and were calculated using the lowest effusion rate of the range – 0.3 m^3/s. If the higher end of the range for lava ridges is used (40 m^3/s), the emplacement times for lava ridges are ~1–11 years. If lava ridges are removed the emplacement times range from ~8 h to 5 years.

6.5. Self-Replicating Lava Flow Model

The self-replication model as outlined by Baloga and Glaze (2008) was applied to 13 qualifying flows to calculate effusion rates and emplacement times as described above. Viscosities were then calculated by treating the lava as a Newtonian fluid and using Jeffrey's equation (Equation 2). Yield strengths were calculated by treating the flow as a Bingham fluid (Equation 4). Modeled effusion rates are ~30–~1,200 m^3/s (Table 4). Eruption rates were highest for lava flows observed in the volcanic plains. Viscosities ranged from 4.5×10^6

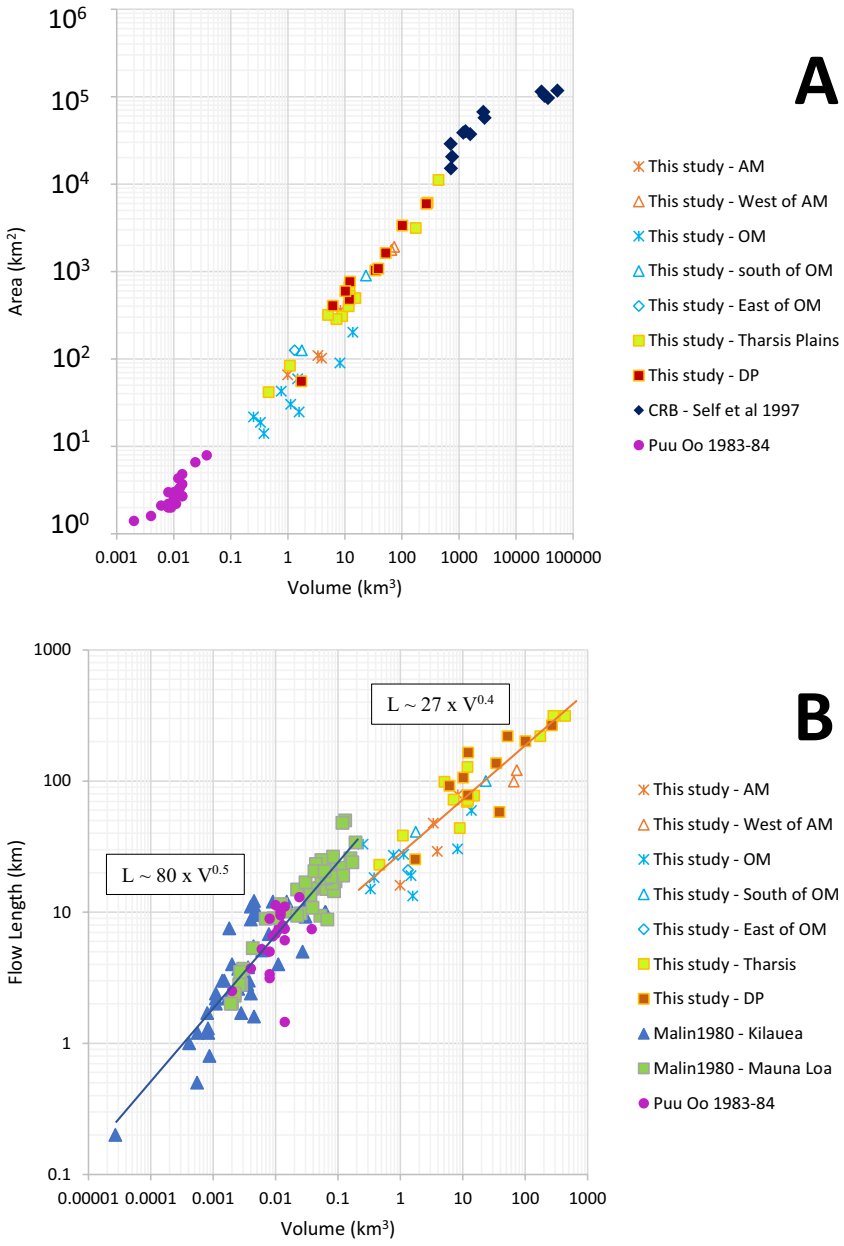

Figure 6. Volumes are expressed as a function of flow length and area covered. AM = Ascraeus Mons; OM = Olympus Mons; DP = Daedalia Planum; CRB = Columbia River Basalts. (a) The calculated volumes and area covered of the 40 lava flows observed in this study are plotted along with the 1983–1984 Pu'u O'o lava flows (Wolfe et al., 1987) and Columbia River Basalt (Self et al., 1997). The smallest flows are not too dissimilar to the Pu'u O'o lava flows, while the largest flows are similar in size and volume to those erupted in the Columbia River basalts. (b) Measured flow length is plotted as a function of calculated volume for 40 lava flows on Mars and are compared to terrestrial flows in Hawai'i. The bulk of Martian flows are longer and volumetrically larger, however, a subset of flows primarily related to central volcanoes overlap in length with Mauna Loa flows. Power law relationships (blue line—terrestrial; orange line—Mars) for Hawaiian lava flows are compared to the Martian lava flows. According to Malin (1980), an exponent equal to 0.5 indicates both length and cross-sectional area of the flows are controlled by volume. The Mars lava flows have an exponent ~0.4 indicating length and cross-sectional area are largely controlled by volume.

Table 2
Eruption Rates and Rheological Properties of 34 Lava Flows on Mars Using a Graetz Number of 300 and Jefferey's Equation

Calculations using Graetz number and Jeffrey's equation							
Flow #	Eruption rate (m^3/s)	Viscosity (Pa-s)	Yield strength (Pa)	Change in eruption rate (G = 230/370)	Change in viscosity (G = 230/370)	Change in yield strength (ρ = −25%/−50%)	Change in viscosity (ρ = −25%/−50%)
1	1.7E+03	9.4×10^4	7.7×10^2	−23%/+23%	+30%/−19%	−26%/−50%	−26%/−50%
2	1.9E+04	2.1×10^6	3.1×10^3	−23%/+23%	+30%/−19%	−26%/−50%	−26%/−50%
3	3.5E+04	9.4×10^5	2.2×10^3	−23%/+23%	+30%/−19%	−26%/−50%	−26%/−50%
4	6.0E+01	7.4×10^7	3.1×10^4	−23%/+23%	+30%/−19%	−26%/−50%	−26%/−50%
5	2.5E+02	1.4×10^6	1.3×10^4	−23%/+23%	+30%/−19%	−26%/−50%	−26%/−50%
6	3.4E+02	3.3×10^7	1.8×10^4	−23%/+23%	+30%/−19%	−26%/−50%	−26%/−50%
7	4.0E+03	7.9×10^5	2.0×10^3	−23%/+23%	+30%/−19%	−26%/−50%	−26%/−50%
8	2.9E+03	1.4×10^5	9.3×10^2	−23%/+23%	+30%/−19%	−26%/−50%	−26%/−50%
9	2.8E+03	1.4×10^6	3.1×10^3	−23%/+23%	+30%/−19%	−26%/−50%	−26%/−50%
10	3.7E+03	2.5×10^6	4.3×10^3	−23%/+23%	+30%/−19%	−26%/−50%	−26%/−50%
11	4.0E+03	6.9×10^6	4.0×10^3	−23%/+23%	+30%/−19%	−26%/−50%	−26%/−50%
12	1.7E+04	4.6×10^6	6.0×10^3	−23%/+23%	+30%/−19%	−26%/−50%	−26%/−50%
13	1.2E+04	9.0×10^5	3.0×10^3	−23%/+23%	+30%/−19%	−26%/−50%	−26%/−50%
14	6.2E+03	1.3×10^6	3.8×10^3	−23%/+23%	+30%/−19%	−26%/−50%	−26%/−50%
15	3.5E+03	1.6×10^5	2.0×10^3	−23%/+23%	+30%/−19%	−26%/−50%	−26%/−50%
16	5.0E+03	1.6×10^5	2.8×10^3	−23%/+23%	+30%/−19%	−26%/−50%	−26%/−50%
17	4.2E+03	2.0×10^5	1.9×10^3	−23%/+23%	+30%/−19%	−26%/−50%	−26%/−50%
18	6.6E+02	9.5×10^5	2.0×10^3	−23%/+23%	+30%/−19%	−26%/−50%	−26%/−50%
19	2.1E+03	1.2×10^6	3.5×10^3	−23%/+23%	+30%/−19%	−26%/−50%	−26%/−50%
20	4.8E+03	3.8×10^6	3.3×10^3	−23%/+23%	+30%/−19%	−26%/−50%	−26%/−50%
21	7.9E+03	3.4×10^6	3.4×10^3	−23%/+23%	+30%/−19%	−26%/−50%	−26%/−50%
22	1.5E+02	1.1×10^7	1.4×10^4	−23%/+23%	+30%/−19%	−26%/−50%	−26%/−50%
23				-			
24	3.0E+02	7.0×10^6	1.5×10^4	−23%/+23%	+30%/−19%	−26%/−50%	−26%/−50%
25							
26							
27							
28							
29							
30	1.6E+03	3.0×10^6	2.3×10^3	−23%/+23%	+30%/−19%	−26%/−50%	−26%/−50%
31	2.5E+02	2.0×10^7	7.5×10^3	−23%/+23%	+30%/−19%	−26%/−50%	−26%/−50%
32	2.3E+03	2.8×10^6	3.4×10^3	−23%/+23%	+30%/−19%	−26%/−50%	−26%/−50%
33	2.2E+03	3.2×10^6	4.1×10^3	−23%/+23%	+30%/−19%	−26%/−50%	−26%/−50%
34	1.6E+03	1.3×10^6	2.8×10^3	−23%/+23%	+30%/−19%	−26%/−50%	−26%/−50%
35	2.9E+03	2.1×10^5	2.2×10^3	−23%/+23%	+30%/−19%	−26%/−50%	−26%/−50%
36	4.0E+02	1.6×10^5	1.3×10^3	−23%/+23%	+30%/−19%	−26%/−50%	−26%/−50%
37	8.2E+02	2.1×10^5	1.7×10^3	−23%/+23%	+30%/−19%	−26%/−50%	−26%/−50%
38	5.2E+03	1.8×10^5	1.7×10^3	−23%/+23%	+30%/−19%	−26%/−50%	−26%/−50%

Table 2
Continued

Calculations using Graetz number and Jeffrey's equation							
Flow #	Eruption rate (m^3/s)	Viscosity (Pa-s)	Yield strength (Pa)	Change in eruption rate ($G = 230/370$)	Change in viscosity ($G = 230/370$)	Change in yield strength ($\rho = -25\%/-50\%$)	Change in viscosity ($\rho = -25\%/-50\%$)
39	3.1E+03	7.0×10^5	1.9×10^3	−23%/+23%	+30%/−19%	−26%/−50%	−26%/−50%
40	8.2E+03	9.7×10^6	5.8×10^3	−23%/+23%	+30%/−19%	−26%/−50%	−26%/−50%

Note. Blank cells represent lava ridges, whose eruption rates cannot be estimated based on their morphology.

to ~3×10^7 Pa s and yield strengths ranged from ~10^3 Pa to 3.6×10^4 Pa. The time of emplacement for these flows ranges from 4.5 months to 9 years. No appreciable difference in viscosity or emplacement time was observed between the Tharsis subregions.

7. Discussion and Implications

7.1. Martian Volcanism

7.1.1. Volumes, Extent, and Distribution of Lava Flows

Martian volcanism has decreased in spatial extent and frequency. According to a number of studies that have used crater counts, geomorphology, and modeling, the bulk of Martian volcanism occurred >3 Ga during the Noachian and Early Hesperian (e.g., Plescia, 2004; Tanaka et al., 2014; Werner, 2009). Early volcanic activity consisted of plains-style volcanism, possible explosive eruptions, and the construction of the large shields (e.g., Carr, 1973, 1974; Plescia, 2004). As Mars has cooled over time, the number of volcanoes erupting and the volumes of erupted magma have decreased (e.g., Bleacher, Greeley, Williams, Cave, & Neukum, 2007; Bleacher, Greeley, Williams, Werner, et al., 2007; Greeley & Spudis, 1981; Werner, 2009; Xiao et al., 2012). The flows in our study are among the most recent examples of effusive volcanism in the Tharsis volcanic province and on Mars. Studies by Tanaka et al. (2014) and Werner (2009) suggest that these flows were emplaced in the Late Amazonian and range in age from 10 to 100s of millions of years old. There is some variability in age among sub-regions within Tharsis. The flows on the flanks of Olympus Mons and Ascraeus Mons are ~100–700 Ma and 100–800 Ma, respectively, with localized areas <50 Ma while the aprons emanating from Ascraeus Mons aprons are ~1 Ga (e.g., Neukum et al., 2004; Werner, 2009), compared to the flows in the volcanic plains that likely range in age from <100 to 400 Ma (e.g., Hauber et al., 2011). The volumes of eruptions are also less on Olympus Mons and the Ascraeus Mons apron relative to the volcanic plains (Bleacher, Greeley, Williams, Cave, & Neukum, 2007; Bleacher, Greeley, Williams, Werner, et al., 2007; this study).

Figure 6a shows the area covered by our flows in km^2 versus their volumes in km^3. It is important to note that these flow area and volume estimates represent minima as the sources of the flows are no longer visible and portions of some flows have been covered by subsequent flows, thus the full length of the flows and areal extent cannot be ascertained. In terms of volume and corresponding area, flows associated with the central volcanoes of Ascreaus Mons (AM) and Olympus Mons (OM) (denoted by stars) are distinct from and smaller than flows associated with plains volcanism (squares). A similar relationship can be seen in Figure 6b where lava flow length (km) is shown against total volume.

In Figure 6a, we also compare the Mars flows to well-documented terrestrial flows. We first note that in terms of volume/area, the Mars flows follow the same trend as terrestrial flows and sit directly between Hawaiian flows (Pu'u O'o, 1983–1984, Wolfe et al., 1987) and flows from the Columbia River Basalts (CRB, Self et al., 1996). Further, the OM and AM flows sit close to the Pu'u O'o flows whereas the plains flows extend over a greater range, reaching but not overlapping with the CRB flows. We also note that the plains flows are longer than flows erupted from central vents (Figure 6b).

In Figure 6b, we note that the relationship between volume and length follows a power law for both terrestrial and Mars flows. The terrestrial flows follow a relationship with a power-law exponent of roughly 0.5. According to Malin (1980), a power-law exponent of 0.33 would indicate that flow length, width, and

Table 3
Eruption Rate Ranges for 40 Lava Flows on Mars by Based on Surface Morphology, Assigned Ψ Value, and Assumed Ambient and Flow Properties

				Application of Ψ			
Flow #	Ψ morphology	Assigned Ψ range	Eruption rates (m^3/s)	Changes in erupted temperature (−50/+50°C)	Changes in erupted density (−50%/−25%)	Changes in ambient temperature (−30/+30°C)	Changes in solidification temperature (−50/+50°C)
1	High (levees)	34–54	1,800–12,000	250%/−33%	(+2/+1)	+28%/−22%	−85%/+844%
2	High (levees)	34–54	1,800–12,000	250%/−33%	(+2/+1)	+28%/−22%	−85%/+844%
3	Very high-high (smooth-levees)	55–59	12,000–18,000	244%/−33%	(+2/+1)	+33%/−20%	−85%/+900%
4	High-intermediate (Levee-Folds)	30–33	1,100–1,800	253%/−33%	(+2/+1)	+27%/−23%	−86%/+810%
5	High-intermediate (levee-folds)	30–33	1,100–1,800	253%/−33%	(+2/+1)	+27%/−23%	−86%/+810%
6	High (levees)	34–54	1,800–12,000	250%/−33%	(+2/+1)	+28%/−22%	−85%/+844%
7	High (levees)	34–54	1,800–12,000	250%/−33%	(+2/+1)	+28%/−22%	−85%/+844%
8	High (levees)	34–54	1,800–12,000	250%/−33%	(+2/+1)	+28%/−22%	−85%/+844%
9	High (levees)	34–54	1,800–12,000	250%/−33%	(+2/+1)	+28%/−22%	−85%/+844%
10	High (levees)	34–54	1,800–12,000	250%/−33%	(+2/+1)	+28%/−22%	−85%/+844%
11	High-intermediate (levee-folds)	30–33	1,100–1,800	253%/−33%	(+2/+1)	+28%/−22%	−86%/+810%
12	High (levees)	34–54	1,800–12,000	250%/−33%	(+2/+1)	+28%/−22%	−85%/+844%
13	High (levees)	34–54	1,800–12,000	250%/−33%	(+2/+1)	+28%/−22%	−85%/+844%
14	High (levees)	34–54	1,800–12,000	250%/−33%	(+2/+1)	+28%/−22%	−85%/+844%
15	High-intermediate (levee-folds)	30–33	1,100–1,800	253%/−33%	(+2/+1)	+27%/−23%	−86%/+810%
16	High (levees)	34–54	1,800–12,000	250%/−33%	(+2/+1)	+28%/−22%	−85%/+844%
17	High (levees)	34–54	1,800–12,000	250%/−33%	(+2/+1)	+28%/−22%	−85%/+844%
18	Intermediate (folds)	13–30	65–1,100	227%/−35%	(+3/+1)	+31%/−15%	−85%/+920%
19	High (levees)	34–54	1,800–12,000	250%/−33%	(+2/+1)	+28%/−22%	−85%/+844%
20	High (levees)	34–54	1,800–12,000	250%/−33%	(+2/+1)	+28%/−22%	−85%/+844%
21	Very high-high (smooth-levees)	55–59	12,000–18,000	244%/−33%	(+2/+1)	+33%/−20%	−85%/+900%
22	High (levees)	34–54	1,800–12,000	250%/−33%	(+2/+1)	+28%/−22%	−85%/+844%
23	Low (ridge)	4–12	0.3–40	260%/−28%	(+2/+1)	+33%/−17%	−83%/+1,000%
24	High (levees)	34–54	1,800–12,000	250%/−33%	(+2/+1)	+28%/−22%	−85%/+844%
25	Low (ridge)	4–12	0.3–40	260%/−28%	(+2/+1)	+33%/−17%	−83%/+1,000%
26	Low (ridge)	4–12	0.3–40	260%/−28%	(+2/+1)	+33%/−17%	−83%/+1,000%
27	Low (ridge)	4–12	0.3–40	260%/−28%	(+2/+1)	+33%/−17%	−83%/+1,000%
28	Low (ridge)	4–12	0.3–40	260%/−28%	(+2/+1)	+33%/−17%	−83%/+1,000%
29	Low (ridge)	4–12	0.3–40	260%/−28%	(+2/+1)	+33%/−17%	−83%/+1,000%
30	High (levees)	34–54	1,800–12,000	250%/−33%	(+2/+1)	+28%/−22%	−85%/+844%
31	High (levees)	34–54	1,800–12,000	250%/−33%	(+2/+1)	+28%/−22%	−85%/+844%
32	High (levees)	34–54	1,800–12,000	250%/−33%	(+2/+1)	+28%/−22%	−85%/+844%
33	High (levees)	34–54	1,800–12,000	250%/−33%	(+2/+1)	+28%/−22%	−85%/+844%
34	High (levees)	34–54	1,800–12,000	250%/−33%	(+2/+1)	+28%/−22%	−85%/+844%
35	High (levees)	34–54	1,800–12,000	250%/−33%	(+2/+1)	+28%/−22%	−85%/+844%
36	High (levees)	34–54	1,800–12,000	250%/−33%	(+2/+1)	+28%/−22%	−85%/+844%
37	High (levees)	34–54	1,800–12,000	250%/−33%	(+2/+1)	+28%/−22%	−85%/+844%
38	High (levees)	34–54	1,800–12,000	250%/−33%	(+2/+1)	+28%/−22%	−85%/+844%

Table 3
Continued

		Application of Ψ					
Flow #	Ψ morphology	Assigned Ψ range	Eruption rates (m^3/s)	Changes in erupted temperature (−50/+50°C)	Changes in erupted density (−50%/−25%)	Changes in ambient temperature (−30/+30°C)	Changes in solidification temperature (−50/+50°C)
39	High (levees)	34–54	1,800–12,000	250%/−33%	(+2/+1)	+28%/−22%	−85%/+844%
40	High (levees)	34–54	1,800–12,000	250%/−33%	(+2/+1)	+28%/−22%	−85%/+844%

Note. Largest sources of uncertainty/error in eruption rates are provided. Ψ is heavily dependent on temperature, whose estimates produces the most uncertainty. Uncertainties for density changes are listed in orders of magnitude.

depth are equally controlled by (and proportional to) the volume erupted, whereas an exponent of 1 would indicate that the cross-sectional area of the flow does not vary with volume, and thus only the length is controlled by volume. Malin (1980) interprets the exponent of 0.5 to indicate that both the length and cross-sectional area (product of thickness and width) of the flows are controlled by the volume, and that length and cross-sectional area are mutually dependent. The Mars flows can be fitted by an exponent close to 0.4, again suggesting that volume controls both length and cross-sectional area, with the <0.5 exponent of the Mars flows probably reflecting the thicker and wider dimensions of the Mars flows relative to their terrestrial counterparts. This is likely a partial effect of Mars' lower gravity. Other possibilities include a wide range of substrate slopes and the viscosities that also control flow geometry in complex ways.

7.1.2. Model Results: Effusion Rate, Duration, and Rheology

Our calculated effusion rates allow differentiation among the subregions (Figure 7a), with the highest rates estimated for the plains regions (squares) and the lowest values estimated for Ascreaus and Olympus Mons (stars). Regions located between central volcanoes and volcanic plains (triangles) have intermediate effusion rates. The application of the halting Graetz number ($G_z = 300$) and the self-replicating model of Baloga and Glaze (2008) produce eruption rates for Ascreaus and Olympus Mons that match well to terrestrial values despite the much greater volumes of the Mars flows (Figures 7b and 7c, orange Xs vs. purple + s). Eruption rates for the plains regions on Mars exceed many Hawaiian eruption rates but are consistent with some of the highest eruption rates measured at the Pu'u O'o vent (1983–1984, Wolfe et al., 1987) and Mauna Loa (1984, Lipman & Banks, 1987). Lower eruption rates are estimated when flow morphology and mass allocation to levees are taken into account in the self-replicating model (Figure 7; Baloga & Glaze, 2008; Glaze & Baloga, 2006). Eruption rates obtained using Ψ morphologies span nearly the entire range of available terrestrial values and those obtained by the two other models, with the exception of the uppermost values calculated by assuming a halting $G_z = 300$. As stated previously, Ψ morphology assigned based on the preserved flow morphology. That value likely represents an average value, as the flow likely transitioned through different regimes along its length and through time. However, the dominant morphology—such as the very long, well-defined channel flows of Tharsis—is a fair indicator of general flow behavior and has been used frequently in the literature when reconstructing flow emplacement.

The flows on Olympus Mons and the Ascraeus Mons apron are smaller in areal extent and shorter than those observed in the volcanic plains of Tharsis and tend to be open channel flows, which may suggest short-lived, volume-limited eruptions (Bleacher, Greeley, Williams, Cave, & Neukum, 2007; Bleacher, Greeley, Williams, Werner, et al., 2007). The variability in flow volume by subregion suggests different eruption conditions, specifically differences in subsurface pathways and magma sources. The volumetrically larger flows were likely erupted to the surface by large dikes and remained active for long periods of time (Figure 8), consistent with findings of Wilson and Head (1983). Meanwhile, the flows on Olympus Mons and proximal to Ascraeus Mons were likely emplaced by smaller subsurface conduits that were active for shorter periods of time consistent with findings of Bleacher, Greeley, Williams, Cave, & Neukum (2007), Bleacher, Greeley, Williams, Werner, et al. (2007), and Wilson and Head (1983). We also note that the largest of the Mars flows, given the measured volumes and calculated eruption rates, must have been active much longer than typical terrestrial flows from places like Hawaii (Figure 8), but may rather be akin to regions like the

Table 4
Eruption Rates and Rheologic Properties of 13 Lava Flows on Mars Using the Self-Replication Model for Long Lava Flows

Self-replication lava flow model (Baloga & Glaze, 2008)							
Flow #	Yield strength (Pa)	Eruption rate (m^3/s)	Viscosity (Pa-s)	Yield strength uncertainty (−50/25% density)	Eruption rate uncertainty (+25% flow length)	Viscosity uncertainty (−25%/+25% core thickness)	Viscosity uncertainty (+25% flow length)
1							
2	3.4×10^3	1,200	9.5×10^6	−50%/−26%	+20%	−44%/+57%	−20%
3	5.3×10^3	340	2.9×10^7	−50%/−26%	+20%	−44%/+57%	−20%
4							
5							
6							
7							
8							
9							
10	4.6×10^3	53	3.2×10^7	−50%/−26%	+20%	−44%/+57%	−20%
11							
12							
13							
14	3.3×10^3	140	2.0×10^7	−50%/−26%	+20%	−44%/+57%	−20%
15							
16							
17							
18							
19							
20							
21	7.9×10^3	290	1.5×10^7	−50%/−26%	+20%	−44%/+57%	−20%
22	1.7×10^4	28	2.9×10^7	−50%/−26%	+20%	−44%/+57%	−20%
23							
24	3.6×10^4	27	1.5×10^7	−50%/−26%	+20%	−44%/+57%	−20%
25							
26							
27							
28							
29							
30	1.4×10^3	46	1.7×10^7	−50%/−26%	+20%	−44%/+57%	−20%
31							
32	2.7×10^3	240	1.6×10^7	−50%/−26%	+20%	−44%/+57%	−20%
33	4.0×10^3	200	2.2×10^7	−50%/−26%	+20%	−44%/+57%	−20%
34	2.0×10^3	51	1.0×10^7	−50%/−26%	+20%	−44%/+57%	−20%
35	2.8×10^3	90	2.5×10^6	−50%/−26%	+20%	−44%/+57%	−20%
36							
37							
38							

Table 4
Continued

Self-replication lava flow model (Baloga & Glaze, 2008)							
Flow #	Yield strength (Pa)	Eruption rate (m^3/s)	Viscosity (Pa-s)	Yield strength uncertainty (−50/25% density)	Eruption rate uncertainty (+25% flow length)	Viscosity uncertainty (−25%/+25% core thickness)	Viscosity uncertainty (+25% flow length)
39	1.4×10^3	110	4.5×10^6	−50%/−26%	+20%	−44%/+57%	−20%
40							

Note. Uncertainty estimates are also included (Baloga & Glaze, 2008).

Columbia River Basalts which are thought to have been active over long periods to generate voluminous fields; this is particularly likely for the Mars plains volcanism characterized here (Self et al., 1996).

7.1.3. Comparison to Previous Work

Our results are generally consistent with other studies: Hiesinger et al. (2007) calculated effusion rates for 25 young flows on the eastern flank of Ascraeus Mons, resulting in a range of ~20–~400 m^3/s, similar to values estimated for the central volcanoes in our study. On the other hand, our effusion rates for the lava ridges, interpreted as tube-fed flows (0.3–40 m^3/s) fall at the very low end of the range proposed by Sakimoto et al. (1997) of 2–10^5 m^3/s. Despite the long runouts of lava flows in the Tharsis region of Mars, our analysis shows that very high effusion rates of ~10^5 m^3/s are not required to explain the observed flows.

Earlier studies of Martian volcanism invoked ultramafic and other exotic compositions to explain the large, voluminous effusive eruptions preserved across the surface of the planet (e.g., Cashman et al., 1998; Garry et al., 2007; Sakimoto et al., 1997). While the ranges differ depending on the model, the viscosities of 10^4–10^7 Pa s calculated in this study are consistent with a basalt to basaltic andesite composition, which is observed on all dust-free Martian surfaces (e.g., Rogers & Christensen, 2007). These viscosities are similar to those calculated for the 25 young lava flows observed (10^4–10^7 Pa s) by Hiesinger et al. (2007) and the 8 lava flows observed in the volcanic plains of Tharsis (102–103 Pa s) by Hauber et al. (2011). The viscosity of some Columbia River Basalt and Deccan Trap lavas has been estimated to be 500 and 100 Pa s at the time of emplacement (e.g., Self et al., 1997, 2008).

The rheologic model results in slightly lower calculated viscosities, due to the estimate of effusion rate (Q) which could be an order of magnitude higher than reality because it assumes the entire flow front is active during the time of emplacement. Jeffrey's equation is particularly sensitive to the flow thickness. The flow thicknesses measured in our study are taken to be the maximum thickness, assuming erosion and gradation has not significantly altered the flow. The self-replication model produces viscosity values at the higher end of basalt (10^6–10^7 Pa s) and more congruent with basaltic andesite or a highly crystallized basalt. Baloga and Glaze (2008) obtained a value of 106 Pa s for one very long lava flow, which is the same flow as our Flow 2, for which we calculated ~107 Pa s. The difference is due to differing flow lengths: Baloga and Glaze (2008) measured a 173 km flow length, whereas we measured 313 km for the same flow.

7.1.4. Implications for the Martian Climate

The contribution of effusive volcanism to climate has been a subject of open speculation for terrestrial and extraterrestrial systems, such that both total mass erupted and eruption duration play a role in controlling climate forcing (Figure 9; Black & Manga, 2017; Rader et al., 2017; Self et al., 1997). Although we acknowledge the differences in the terrestrial and Martian atmospheres, we do think it worthy of a thought-provoking exercise to bridge the terrestrial and planetary communities. Some of the eruptions represented by the lava flows in our study may have lasted for years or decades and the masses are on the order of very large terrestrial eruptions. The masses of individual flows calculated in our study are less than that of complete members in terrestrial large igneous provinces, but some calculated masses, especially those in the volcanic plains, do overlap with other eruptions that had significant global impacts on Earth, consistent with up to 2° of global cooling. While large igneous provinces typically erupt over millions of years on Earth, the Tharsis

Figure 7. AM = Ascraeus Mons; OM = Olympus Mons; DP = Daedalia Planum. (a) Relationship between eruption rate and area covered. The Mars flows are compared to flows erupted during the 1983–1984 Pu'u O'o eruption in Hawai'i (Wolfe et al., 1987) and the Columbia River Basalts (CRB). Large symbols denote values derived using self-replication model for long lava flows. Small symbols indicate values calculated using Graetz number. Stars indicate values obtained for central volcanoes. Navy blue line denotes minimum areal extent of CRB flows from Self et al. (1997). This data supports the conclusion that eruption rates are controlled by subregions, with higher eruption rates calculated for the volcanic plains than central volcanoes. In general, the self-replication model produces lower eruption rates than using the Graetz number. (b) The relationship between eruption rate and total erupted volume. The eruption rates for the Mars lava flows are comparable to terrestrial values. The highest eruption rates calculated for Mars are similar to the highest values observed on Earth during the Mauna Loa eruption of 1984. Although the lower volume estimates are similar to those observed on Mauna Loa, most of the flow volumes are 2–4 orders of magnitude greater. (c) Figure modified from Walker (1973). Log-log plot shows the length of lava flows as function of the eruption rate for terrestrial lava flows at Mauna Loa and Kilauea. Superposed on that figure are the eruption rates calculated using the three models in this study. Orange X's are calculated eruption rates using Graetz number. Purple +'s are eruption rates calculated from self-replication model. Shaded gray box represents ranges of eruption rates calculated using Ψ.

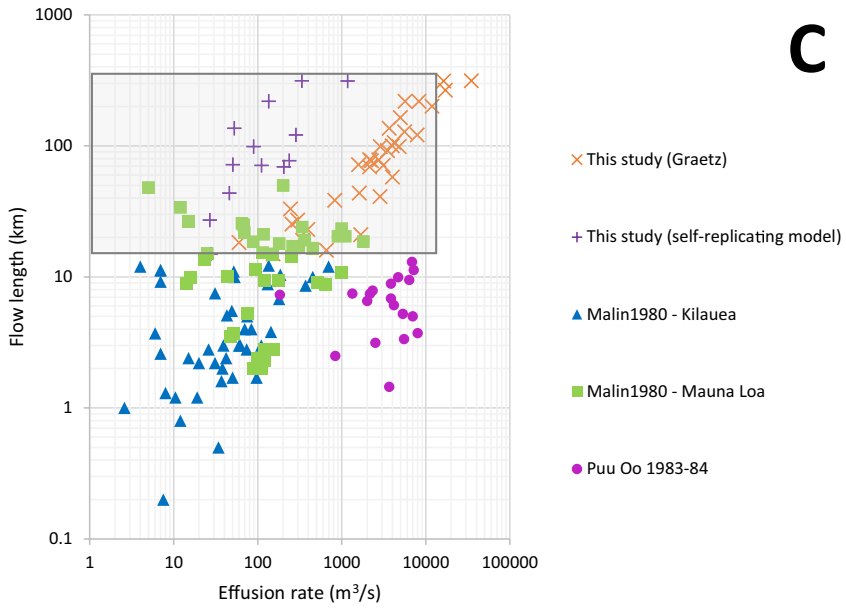

Figure 7. *Continued*

volcanic province has produced volcanic eruptions over billions of years (e.g., Self et al., 1996, 1997, 2008; Sheth, 2006; Tanaka et al., 2014; Werner, 2009), possibly enhancing their capacity for atmospheric forcing. And, the high altitude of the eruptions at Tharsis may have further enhanced their ability to produce climat-

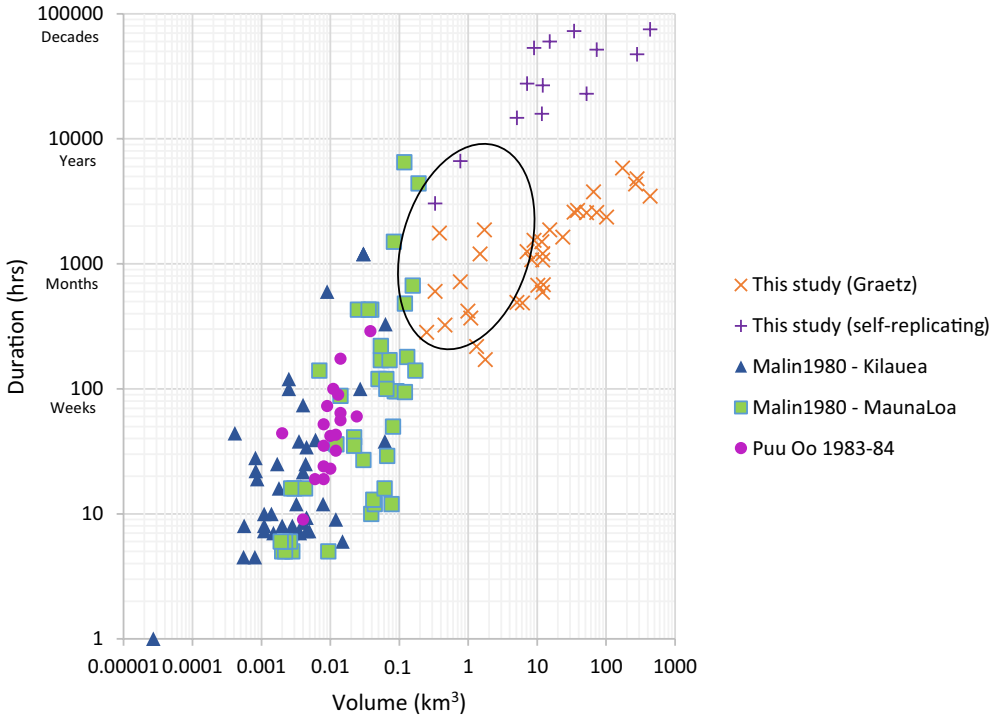

Figure 8. The calculated volume of Mars lava flows is compared to terrestrial flows as a function of duration of emplacement. Black circle contains Mars flows associated with central volcanoes, whereas remaining flows were produced in the plains. The Mars lava flows are much larger in volume—although some values are similar to Mauna Loa—and erupted over greater lengths of time. This suggests that feeder dikes and other pathways necessary to producing these flows remained active and open for longer periods than pathways on Earth.

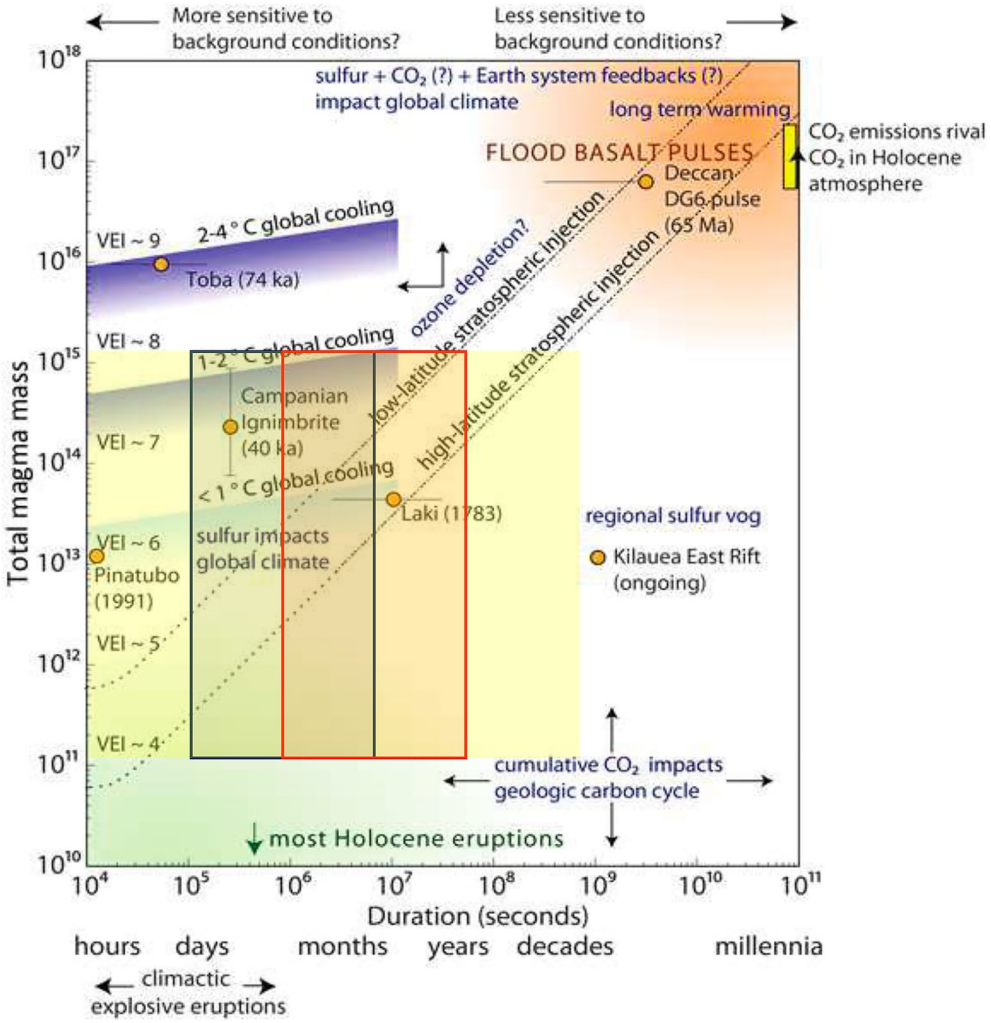

Figure 9. Mass of observed Martian flows and emplacement times are compared with notable terrestrial eruptions. Blue box represents Graetz number minimum eruption durations, while red box represents self-replication model eruption durations. Yellow box represents eruption durations for full range of Ψ derived eruption rates. While the Martian and terrestrial atmospheres are wholly different, it is intriguing to speculate on the potential impacts of the mass of observed material erupted in this study. Modified from Black and Manga (2017).

ic impacts (e.g., Sheth, 2006). Whether or not those eruptions were continuous or volumetrically significant enough to impact the atmosphere remains an open question, although our analysis demonstrates that individual flows in Tharsis are at the very least of the scale of large terrestrial eruptions that caused short term changes to global climate.

8. Conclusions

This study produced volumes, effusion rates, viscosities, and emplacement times for 40 lava flows in the Tharsis volcanic province on Mars. The results have direct implications for recent volcanism on Mars, lava composition, and the plumbing of the Martian subsurface. Sub-regional differences in flow volumes across the Tharsis volcanic province suggest different magma sources and subsurface plumbing conditions for central volcanoes and lava plains. Drawing from these analyses, we conclude the following:

1. The lava flows observed in this study are of considerable area and volume relative to typical terrestrial lava flows. Some of the larger lava flows are similar in magnitude to flows, or sequences of flows, erupted

in Large Igneous Provinces. In general, these lava flows are thicker and/or wider for a given length than terrestrial flows.
2. The lava flows observed in this study do not require extremely high volumetric flow rates or exotic lava compositions. The observed lava flows can be produced by volumetric flow rates at the higher end of documented terrestrial values and nonexotic lava compositions with viscosities and yield strengths suggestive of basalt and basaltic andesite compositions.
3. A key difference between the observed Martian lava flows and terrestrial flows is the longer-lived eruptions capable of producing individual lava flows of remarkable length and volume in relatively recent Martian history.
4. Olympus Mons has produced volumetrically smaller eruptions than the sources of lava flows in the volcanic plains, suggesting either shorter lived eruptions, smaller dikes, and/or a smaller magma source.

Data Availability Statement

Data sets for this research are archived in the ASU Library Digital Repository and are included in this paper (and its Supplementary Information files): Peters (2020) (https://search.lib.asu.edu/permalink/01ASU_INST/1o1u1i6/alma991048581851403841).

Acknowledgments
This work was supported by a NASA/JPL THEMIS contract 1228404. NASA spacecraft data used in this study are referred to in the Methods section of this paper. This manuscript was greatly improved thanks to constructive feedback from an anonymous reviewer and Steve Baloga.

References

Baloga, S. M., & Glaze, L. S. (2008). A self-replication model for long channelized lava flows on the Mars plains. *Journal of Geophysical Research*, *113*, E05003. https://doi.org/10.1029/2007JE002954

Baloga, S. M., Glaze, L. S., Crisp, J. A., & Stockman, S. A. (1998). New statistics for estimating the bulk rheology of active lava flows: Puu Oo examples. *Journal of Geophysical Research*, *103*(B3), 5133–5142. https://doi.org/10.1029/97jb03743

Belousov, A., Belousov, M., Edwards, B., Volynets, A., & Melnikov, D. (2015). Overview of the precursors and dynamics of the 2012–13 basaltic fissure eruption of Tolbachik Volcano, Kamchatka, Russia. *Journal of Volcanology and Geothermal Research*, *307*, 22–37. https://doi.org/10.1016/j.jvolgeores.2015.04.009

Black, B. A., & Manga, M. (2016). The eruptibility of magmas at Tharsis and Syrtis Major on Mars. *Journal of Geophysical Research: Planets*, *121*, 944–964. https://doi.org/10.1002/2016JE004998

Black, B. A., & Manga, M. (2017). Volatiles and the tempo of flood basalt magmatism. *Earth and Planetary Science Letters*, *458*, 130–140. https://doi.org/10.1016/j.epsl.2016.09.035

Blake, S., & Bruno, B. C. (2000). Modelling the emplacement of compound lava flows. *Earth and Planetary Science Letters*, *184*, 181–197.

Bleacher, J. E., Greeley, R., Williams, D. A., Cave, S. R., & Neukum, G. (2007). Trends in effusive style at the Tharsis Montes, Mars, and implications for the development of the Tharsis province. *Journal of Geophysical Research*, *112*, E09005. https://doi.org/10.1029/2006JE002873

Bleacher, J. E., Greeley, R., Williams, D. A., Werner, S. C., Hauber, E., & Neukum, G. (2007). Olympus Mons, Mars: Inferred changes in late Amazonian aged effusive activity from lava flow mapping of Mars Express High-Resolution Stereo data. *Journal of Geophysical Research*, *112*, E04003. https://doi.org/10.1029/2006JE002826

Bleacher, J. E., Orr, T. R., Wet, de, A. P., Zimbelman, J. R., Hamilton, C. W., Garry, W. B., et al. (2017). Plateaus and sinuous ridges as the fingerprints of lava flow inflation in the Eastern Tharsis Plains of Mars. *Journal of Volcanology and Geothermal Research*, *342*, 29–46. https://doi.org/10.1016/j.jvolgeores.2017.03.025

Bruno, B. C., Baloga, S. M., & Taylor, G. J. (1996). Modeling gravity-driven flows on an inclined plane. *Journal of Geophysical Research*, *101*(B5), 11565–11577. https://doi.org/10.1029/96jb00178

Byrne, P. K., Vries, van Wyk de, B., Murray, J. B., & Troll, V. R. (2012). A volcanotectonic survey of Ascraeus Mons, Mars. *Journal of Geophysical Research*, *117*, E01004. https://doi.org/10.1029/2011JE003825

Carr, M. H. (1973). Volcanism on Mars. *Journal of Geophysical Research*, *78*, 4049–4062. https://doi.org/10.1029/jb078i020p04049

Carr, M. H. (1974). Tectonism and volcanism of the Tharsis region of Mars. *Journal of Geophysical Research*, *79*(26), 3942–3949. https://doi.org/10.1029/jb079i026p03943

Cashman, K., Pinkerton, H., & Stephenson, J. (1998). Introduction to special section: Long lava flows. *Journal of Geophysical Research*, *103*(B11), 27281–27289. https://doi.org/10.1029/98jb01820

Cashman, K. V., Kerr, R. C., & Griffiths, R. W. (2006). A laboratory model of surface crust formation and disruption on lava flows through non-uniform channels. *Bulletin of Volcanology*, *68*, 753–770. https://doi.org/10.1007/s00445-005-0048-z

Chemical Rubber Company (CRC). (1984). *CRC handbook of chemistry and physics* (65th ed.). CRC Press, Inc.

Christensen, P. R. (1986). Regional dust deposits on mars: Physical properties, age, and history. *Journal of Geophysical Research*, *91*(B3), 3533–3545. https://doi.org/10.1029/jb091ib03p03533

Christensen, P. R., Jakosky, B. M., Kieffer, H. H., Malin, M. C., McSween, H. Y., Nealson, K., et al. (2004). The Thermal Emission Imaging System (THEMIS) for the Mars 2001 Odyssey mission. *Space Science Reviews*, *110*, 85–130. https://doi.org/10.1023/b:spac.0000021008.16305.94

Crane Company. (1988). *Flow of fluids through valves, fittings, and pipe* (Technical Paper No. 410 (TP 410)).

Crisp, J., & Baloga, S. (1994). Influence of crystallization and entrainment of cooler material on the emplacement of basaltic aa lava flows. *Journal of Geophysical Research*, *99*(B6), 11819–11831. https://doi.org/10.1029/94jb00134

Crown, D. A., & Ramsey, M. S. (2016). Morphologic and thermophysical characteristics of lava flows southwest of Arsia Mons, Mars. *Journal of Volcanology and Geothermal Research*, *342*, 13–28. https://doi.org/10.1016/j.volgeores.2016.07.008

Crumpler, L. S., & Aubele, J. C. (1978). Structural evolution of Arsia Mons, Pavonis Mons, and Ascraeus Mons: Tharsis region of Mars. *Icarus*, *34*, 496–511. https://doi.org/10.1016/0019-1035(78)90041-6

Danes, Z. F. (1972). Dynamics of lava flows. *Journal of Geophysical Research*, *77*(8), 1430–1432.

Fink, J. H., & Griffiths, R. W. (1990). Radial spreading of viscous-gravity currents with solidifying crust. *Journal of Fluid Mechanics*, *221*, 485–509. https://doi.org/10.1017/s0022112090003640

Fink, J. H., & Griffiths, R. W. (1992). A laboratory analogue study of the surface morphology of lava flows extruded from point and line sources. *Journal of Volcanology and Geothermal Research*, *54*, 19–32.

Fink, J. H., Park, S. O., & Greeley, R. (1983). Cooling and deformation of sulfur flows. *Icarus*, *56*, 38–50. https://doi.org/10.1016/0019-1035(83)90126-4

Garry, W. B., Zimbelman, J. R., & Gregg, T. K. P. (2007). Morphology and emplacement of a long-channeled lava flow near Ascraeus Mons volcano, Mars. *Journal of Geophysical Research*, *112*, E08007. https://doi.org/10.1029/2006JE002803

Giacomini, L., Carli, C., Sgavetti, M., & Massironi, M. (2012). Spectral analysis and geological mapping of the Daedalia Planum lava field (Mars) using OMEGA data. *Icarus*, *220*, 679–693. https://doi.org/10.1016/j.icarus.2012.06.010

Giacomini, L., Massironi, M., Martellato, E., Pasquare, G., Frigeri, A., & Cremonese, G. (2009). Inflated flows on Daedalia Planum (Mars)? Clues from a comparative analysis with the Payen volcanic complex (Argentina). *Planetary and Space Science*, *57*, 556–570. https://doi.org/10.1016/j.pss.2008.12.001

Glaze, L. S., & Baloga, S. M. (2006). Rheologic inferences from the levees of lava flows on Mars. *Journal of Geophysical Research*, *111*, E09006. https://doi.org/10.1029/2005JE002585

Glaze, L. S., Baloga, S. M., Garry, W. B., Fagents, S. A., & Parchetta, C. (2009). A hybrid model for leveed lava flows: Implications for eruption styles on Mars. *Journal of Geophysical Research*, *114*, E07001. https://doi.org/10.1029/2008JE003278

Glaze, L. S., Baloga, S. M., & Stofan, E. R. (2003). A methodology for constraining lava flow rheologies with MOLA. *Icarus*, *165*, 26–33. https://doi.org/10.1016/S0019-1035(03)00171-4

Gorelick, N. S., Weiss-Malik, M., Steinber, B., & Anwar, S. (2003). *JMARS: A multimission data fusion applciation*. 34th Lunar and planetary science Conference. Abstract no. 2057.

Greeley, R. (1982). The Snake River Plain, Idaho: Representative of a new category of volcanism, volcanism in Hawaii. *Journal of Geophysical Research*, *87*(B4), 2705–2712.

Greeley, R., & Spudis, P. D. (1981). Volcanism on Mars. *Reviews of Geophysics and Space Physics*, *19*(1), 13–41. https://doi.org/10.1029/rg019i001p00013

Gregg, T. K. P., & Fink, J. H. (1996). Quantification of extraterrestrial lava flow effusion rates through laboratory simulations. *Journal of Geophysical Research*, *101*(E7), 16891–16900. https://doi.org/10.1029/96je01254

Gregg, T. K. P., & Fink, J. H. (2000). A laboratory investigation into the effects of slope on lava flow morphology. *Journal of Volcanology and Geothermal Research*, *96*, 145–159. https://doi.org/10.1016/s0377-0273(99)00148-1

Gregg, T. K. P., & Keszthelyi, L. P. (2004). The emplacement of pahoehoe toes: Field observations and comparison to laboratory simulations. *Bulletin of Volcanology*, *66*, 381–391. https://doi.org/10.1007/s00445-003-0319-5

Griffiths, R. W., & Fink, J. H. (1992). The morphology of lava flows in planetary environments: Predictions from analog experiments. *Journal of Geophysical Research*, *97*(B13), 19739–19748. https://doi.org/10.1029/92jb01953

Guest, J. E., Kilburn, C. R. J., Pinkerton, H., & Duncan, A. M. (1987). The evolution of lava flow-fields: Observations of the 1981 and 1983 eruptions of Mount Etna, Sicily. *Bulletin of Volcanology*, *49*, 527–540. https://doi.org/10.1007/bf01080447

Hallsworth, M. A., Huppert, H. E., & Sparks, R. S. J. (1987). A laboratory simulation of basaltic lava flows. *Modern Geology*, *11*, 93–107.

Harris, A. J. L., & Rowland, S. K. (2001). FLOWGO: A kinematic thermo-rheological model for lava flowing in a channel. *Bulletin of Volcanology*, *63*, 20–44. https://doi.org/10.1007/s004450000120

Harris, A. J. L., & Rowland, S. K. (2015). Lava flows and rheology. In The encyclopedia of volcanoes (2nd ed., pp. 321–342). https://doi.org/10.1016/b978-0-12-385938-9.00017-1

Hauber, E., Broz, P., Jagert, F., Jodlowski, P., & Platz, T. (2011). Very recent and wide-spread basaltic volcanism on Mars. *Geophysical Research Letters*, *38*, L10201. https://doi.org/10.1029/2011GL047310

Hiesinger, H., Head, J. W., III, & Neukum, G. (2007). Young lava flows on the eastern flank of Ascraeus Mons: Rheological properties derived from High Resolution Stereo Camera (HRSC) images and Mars Orbiter Laser Altimeter (MOLA) data. *Journal of Geophysical Research*, *112*, E05011. https://doi.org/10.1029/2006JE002717

Hon, K., Kauahikaua, J., Denliger, R., & Mackay, K. (1994). Emplacmenet and inflation of pahoehoe sheet flows: Observations and measurements of active lava flows of Kilauea volcano, Hawaii. *The Geological Society of America Bulletin*, *106*, 351–370. https://doi.org/10.1130/0016-7606(1994)106<0351:eaiops>2.3.co;2

Hulme, G. (1974). The interpretation of lava flow morphology. *Geophysical Journal of the Royal Astronomical Society*, *39*, 361–383. https://doi.org/10.1111/j.1365-246x.1974.tb05460.x

Hulme, G. (1976). The determination of the rheological properties and effusion rate of an Olympus Mons Lava. *Icarus*, *27*, 207–213. https://doi.org/10.1016/0019-1035(76)90004-x

Hulme, G., & Fielder, G. (1977). Effusion rates and rheology of lunar lavas. *Philosophical Transactions of the Royal Society of London A*, *285*, 227–234. https://doi.org/10.1098/rsta.1977.0059

Jaeger, W. L., Keszthelyi, K. P., Skinner, J. A., Jr., Milazzo, M. P., McEwen, A. S., Titus, T. N., et al. (2010). Emplacement of the youngest flood lava on Mars: A short, turbulent story. *Icarus*, *205*, 230–243. https://doi.org/10.1016/j.icarus.2009.09.011

Jaumann, R., Neukum, G., Behnke, T., Duxbury, T. C., Eichentopf, K., Flohre, J., et al. (2007). The high-resolution stereo camera (HRSC) experiment on Mars Express: Instrument aspects and experiment conduct from interplanetary cruise through the nominal mission. *Planetary and Space Science*, *55*, 928–952. https://doi.org/10.1016/j.pss.2006.12.003

Jeffreys, H. (1925). The flow of water in an inclined channel of rectangular section. *The London, Edinburgh, and Dublin Philosophical Magazine and Journal of Science*, *49*(293), 793–807. https://doi.org/10.1080/14786442508634662

Keszthelyi, L., Jaegar, W., McEwen, A., Tornabene, L., Beyer, R. A., Dundas, C., & Milazzo, M. (2008). High Resolution Imaging Science Experiment (HiRISE) images of volcanic terrains from the first 6 months of the Mars Reconnaissance Orbiter Primary Science Phase. *Journal of Geophysical Research*, *113*, E04005. https://doi.org/10.1029/2007JE002968

Keszthelyi, L., Thordarson, T., McEwen, A., Haack, H., Guilbaud, M.-N., Self, S., & Rossi, M. J. (2004). Icelandic analogs to Martian flood lavas. *Geochemistry, Geophysics, Geosystems*, *5*, Q11014. https://doi.org/10.1029/2004GC000758

Lipman, P. W., & Banks, N. G. (1987). AA flow dynamics, Mauna Loa. In Volcanism in Hawai'i (pp. 1527–1567).

Malin, M. C. (1980). Lengths of Hawaiian lava flows. *Geology*, *8*, 306–308.

Malin, M. C., Bell, J. F., Cantor, B. A., Caplinger, M. A., Calvin, W. M., Clancy, R. T., et al. (2007). Context camera investigation on board the Mars Reconnaissance Orbiter. *Journal of Geophysical Research*, *112*, E05S04. https://doi.org/10.1029/2006JE002808

McEwen, A. S., Eliason, E. M., Bergstrom, J. W., Bridges, N. T., Hansen, C. J., Delamere, W. A., et al. (2007). Mars Reconnaissance Orbiter's High-Resolution Imaging Science Experiment (HiRISE). *Journal of Geophysical Research*, *112*, E05S02. https://doi.org/10.1029/2005JE002605

Moore, H. J., Arthur, D. W. G., & Schaber, G. G. (1978). *Yield strengths of flows on the Earth, Mars, and Moon* (pp. 3351–3378). Proceedings of the 9th Lunar and Planetary Science Conference.

NASA Mars Fact Sheet. (2020), *NASA Mars Fact Sheet*. updated 25 November 2020.

Neukum, G., Jaumann, R., Hoffmann, H., Hauber, E., Head, J. W., Basilevsky, A. T., et al. (2004). Recent and episodic volcanic and glacial activity on Mars revealed by the High-Resolution Stereo Camera. *Nature*, *432*, 971–979.

Nichols, R. L. (1939). Viscosity of lava. *The Journal of Geology*, *47*(3), 290–302. https://doi.org/10.1086/624778

Pasckert, J. H., Hiesinger, H., & Reiss, D. (2012). Rheologies and ages of lava flows on Elysium Mons, Mars. *Icarus*, *219*, 443–457. https://doi.org/10.1016/j.icarus.2012.03.014

Peck, D. L. (1978). *Cooling and vesiculation of Alae Lava Lake, Hawai'i*. Geological Survey Professional Paper 935-B.

Peiterson, M. N., & Crown, D. A. (1999). Downflow width behavior of Martian and terrestrial lava flows. *Journal of Geophysical Research*, *104*(E4), 8473–8488. https://doi.org/10.1002/jgre.v104.e4

Peters, S. I. (2020). *Investigating lava flow emplacement: Implications for volcanic Hazards and planetary evolution* (Thesis). Arizona State University, ProQuest Dissertations Publishing.

Peters, S. I., & Christensen, P. R. (2017). Flank vents and graben as indicators of Late Amazonian volcanotectonic activity on Olympus Mons. *Journal of Geophysical Research: Planets*, *112*, 501–523. https://doi.org/10.1002/2016JE005108

Pieri, D. C., Baloga, S. M., Nelson, R. M., & Sagan, C. (1984). Sulfur flows of Ra Patera, IO. *Icarus*, *60*, 685–700. https://doi.org/10.1016/0019-1035(84)90173-8

Pinkerton, H. (1987). Factors affecting the morphology of lava flows. *Endeavour New Series*, *11*(2), 73–79. https://doi.org/10.1016/0160-9327(87)90241-9

Pinkerton, H., James, M., & Jones, A. (2002). Surface measurements of active lava flows on Kilauea volcano, Hawai'i. *Journal of Volcanology and Geothermal Research*, *113*, 159–176. https://doi.org/10.1016/s0377-0273(01)00257-8

Pinkerton, H., & Sparks, R. S. J. (1976). The 1975 Sub-terminal lavas, Mount Etna: A case history of the formation of a compound lava field. *Journal of Volcanology and Geothermal Research*, *1*, 167–182. https://doi.org/10.1016/0377-0273(76)90005-6

Plescia, J. B. (2004). Morphometric properties of Martian volcanoes. *Journal of Geophysical Research*, *109*, E03003. https://doi.org/10.1029/2002JE002031

Rader, E., Vanderkluysen, L., & Clarke, A. (2017). The role of unsteady effusion rates on inflation in long-lived lava flow fields. *Earth and Planetary Science Letters*, *477*, 73–83. https://doi.org/10.1016/j.epsl.2017.08.016

Rogers, A. D., & Christensen, P. R. (2007). Surface mineralogy of Martian low-albedo regions from MGS-TES data: Implications for upper crustal evolution and surface alteration. *Journal of Geophysical Research*, *112*, E01003. https://doi.org/10.1029/2006JE002727

Rowland, S. K., Harris, A. J. L., & Garbeil, H. (2004). Effects of Martian conditions on numerically modeled, cooling-limited, channelized lava flows. *Journal of Geophysical Research*, *109*, E10010. https://doi.org/10.1029/2004JE002288

Sakimoto, S. E. H., Crips, J., & Baloga, S. M. (1997). Eruption constraints on tube-fed planetary lava flows. *Journal of Geophysical Research*, *102*(E3), 6597–6613. https://doi.org/10.1029/97je00069

Scott, D. H., & Tanaka, K. L. (1981). Mars: Paleostratigraphic restoration of buried surfaces in Tharsis Montes. *Icarus*, *45*, 304–319. https://doi.org/10.1016/0019-1035(81)90036-1

Self, S., Jay, A. E., Widdowson, M., & Keszthelyi, L. P. (2008). Correlation of the Deccan and Rajahmundry Trap lavas: Are these the longest and largest lava flows on Earth? *Journal of Volcanology and Geothermal Research*, *172*, 3–19. https://doi.org/10.1016/j.jvolgeores.2006.11.012

Self, S., Thordarson, T., & Keszthelyi, L. (1997). Emplacement of continental flood basalt lava flows. In J. J. Mahoney & M. F. Coffin (Eds.), Large igneous provinces: Continental, oceanic, and planetary flood volcanism (Geophysical Monograph Series, Vol. 100, pp. 381–410).

Self, S., Thordarson, T., Keszthelyi, L., Walker, G. P. L., Hon, K., Murphy, M. T., et al. (1996). A new model for the emplacement of Colombia River basalts as large, inflated pahoehoe lava flow fields. *Geophysical Research Letters*, *23*(19), 2689–2692. https://doi.org/10.1029/96gl02450

Sheth, H. C. (2006). The emplacement of pahoehoe lavas on Kilauea and in the Deccan Traps. *Journal of Earth System Science*, *115*, 615–629. https://doi.org/10.1007/s12040-006-0007-x

Soule, S. A., & Cashman, K. V. (2004). The mechanical properties of solidified polyethylene glycol 600, an analog for lava crust. *Journal of Volcanology and Geothermal Research*, *129*, 139–153. https://doi.org/10.1016/s0377-0273(03)00237-3

Spudis, P. D., McGovern, P. J., & Kiefer, W. S. (2013). Large shield volcanoes on the Moon. *Journal of Geophysical Research: Planets*, *118*, 1063–1081. https://doi.org/10.1002/jgre.20059

Tanaka, K. L., Skinner, J. A., Jr., Dohm, J. M., Irwin, R. P., III, Kolb, E. J., Fortezzo, C. M., et al. (2014). *Geologic map of Mars*. United States Geological Survey.

Vicari, A., Alexis, H., Del Negro, C., Coltelli, M., Marsella, M., & Proietti, C. (2007). Modelling of the 2001 lava flow at Etna volcano by cellular automata approach. *Environmental Modelling & Software*, *22*, 1465–1471. https://doi.org/10.1016/j.envsoft.2006.10.005

Walker, G. P. L. (1971). Compound and simple lava flows and flood basalts. *Bulletin of Volcanology*, *35*, 579–590. https://doi.org/10.1007/bf02596829

Walker, G. P. L. (1973). Lengths of lava flows. *Philosophical Transactions of the Royal Society of London A*, *274*, 107–118. https://doi.org/10.1098/rsta.1973.0030

Werner, S. C. (2009). The global martian volcanic evolutionary history. *Icarus*, *201*, 44–68. https://doi.org/10.1016/j.icarus.2008.12.019

Wilson, L., & Head, J. W., III (1983). A comparison of volcanic eruption processes on Earth, Moon, Mars, Io, and Venus. *Nature*, *302*, 663–669. https://doi.org/10.1038/302663a0

Wolfe, E. W., Garcia, M. O., Jackson, D. B., Koyanagi, R. Y., Neal, C. A., & Okamura, A. T. (1987). *The Pu'u O'o eruption of Kilauea volcano, episodes 1–20, January 3, 1983, to June 8, 1984* (pp. 471–508).

Xiao, L., Huang, J., Christensen, P. R., Greeley, R., Williams, D. A., Zhao, J., & He, Q. (2012). Ancient volcanism and its implication for thermal evolution of Mars. *Earth and Planetary Science Letters*, *323–324*, 9–18. https://doi.org/10.1016/j.epsl.2012.01.027

Zuber, M. T., Smith, D. E., Solomon, S. C., Muhleman, D. O., Head, J. W., Garvin, J. B., et al. (1992). The Mars observer laser altimeter investigation. *Journal of Geophysical Research*, *97*, 7781–7797. https://doi.org/10.1029/92je00341